Gut-specific histamine 3 receptor signaling orchestrates microglia-dependent resolution of peripheral inflammation

Kerstin Dürholz [1,2], Leona Ehnes [1,2], Mathias Linnerbauer [2,3], Eva Schmid [1,2], Heike Danzer [1,2], Michael Hinzpeter-Schmidt[1,2], Lena Lößlein [3], Lena Amend [4], Michael Frech [1,2], Vugar Azizov [1,2], Fabian Schälter [1,2], Arne Gessner [5], Sébastien Lucas [1,2], Till-Robin Lesker [4], R. Verena Taudte [5,6], Jörg Hofmann [7], Felix Beyer [8], Hadar Bootz-Maoz [9], Yasmin Reich [9], Hadar Romano [9], Daniele Mauro [10], Ruth Beckervordersandforth [8], Maja Skov Kragsnaes [11,12], Torkell Ellingsen [12], Wei Xiang [13], Aiden Haghikia [14], Cezmi A. Akdis [15], Francesco Ciccia [10], Tobias Bäuerle [16], Kerstin Sarter [1,2], Till Strowig [4], Nissan Yissachar [9], Georg Schett [1,2], Veit Rothhammer [2,3], Mario M. Zaiss [1,2*]

1 Department of Internal Medicine 3, Rheumatology and Immunology, Friedrich-Alexander-Universität Erlangen-Nürnberg (FAU) and Universitätsklinikum Erlangen, Erlangen, Germany.

2 Deutsches Zentrum Immuntherapie (DZI), Friedrich-Alexander-Universität Erlangen-Nürnberg (FAU) and Universitätsklinikum Erlangen, Erlangen, Germany

3 Department of Neurology, Universitätsklinikum Erlangen, Friedrich-Alexander-Universität Erlangen-Nürnberg (FAU), 91054 Erlangen, Germany.

4 Department of Microbial Immune Regulation, Helmholtz Centre for Infection Research, Braunschweig, Germany; Hannover Medical School, Hannover, Germany.

5 Institute of Experimental and Clinical Pharmacology and Toxicology, Friedrich-Alexander University (FAU) Erlangen-Nürnberg, Erlangen, Germany

6 Core Facility for Metabolomics, Philipp University Marburg, Marburg, Germany

7 Department of Biology, Division of Biochemistry, Friedrich-Alexander University (FAU), 91058 Erlangen, Germany

[8] Institute of Biochemistry, Friedrich-Alexander University of Erlangen-Nürnberg, Erlangen, Germany

[9] The Goodman Faculty of Life Sciences, and Bar-Ilan Institute of Nanotechnology and Advanced Materials, Bar-Ilan University, Ramat-Gan, 5290002, Israel

[10] Department of Precision Medicine, University of Campania "Luigi Vanvitelli", Naples, Italy

[11] Department of Rheumatology, Odense University Hospital, Odense, Denmark

[12] Department of Clinical Research, University of Southern Denmark, Odense, Denmark

[13] Department of Molecular Neurology, University Hospital Erlangen, Friedrich-Alexander-Universität Erlangen-Nürnberg (FAU), Germany

[14] Department of Molecular Cell Biology, Institute of Biochemistry and Pathobiochemistry, Ruhr University Bochum, Bochum 44801, Germany.

[15] Swiss Institute of Allergy and Asthma Research (SIAF), University of Zurich, Davos, Switzerland

[16] Radiologisches Institut, Universitätsklinikum Erlangen, Friedrich-Alexander-Universität Erlangen-Nürnberg, Erlangen, Germany.

Short title: Gut-CNS-joint axis resolves peripheral inflammation.

Keywords: histamine, microglia, gut-joint axis, gut-brain axis, gut-CNS-joint axis, resolution

* Mario M. Zaiss, Department of Internal Medicine 3, University of Erlangen-Nürnberg, Universitätsstrasse 25A, 91054 Erlangen, Germany, Telephone number: +49 9131 85-33794. Fax number: +49 9131 85-34770. mario.zaiss@uk-erlangen.de

The authors have declared that no conflict of interest exists.

Graphical Abstract

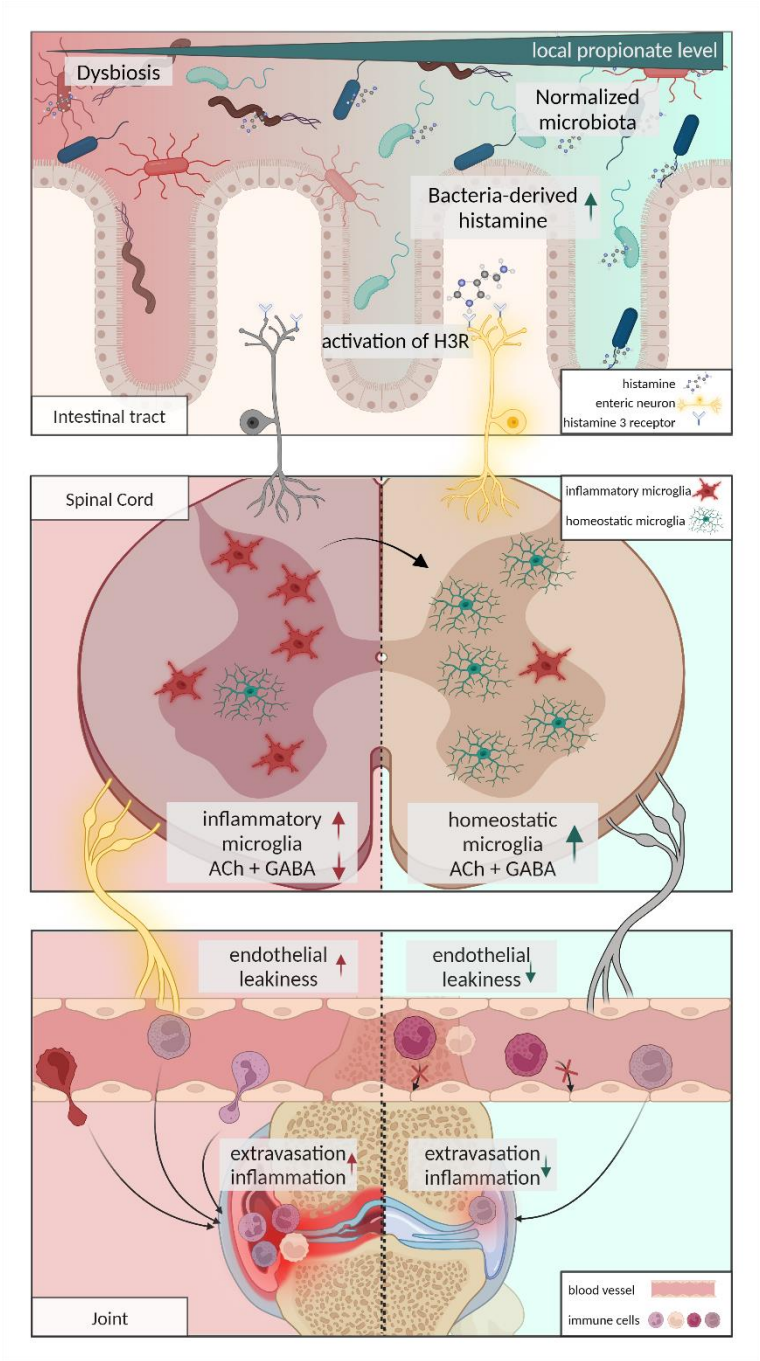

Abstract

Chronic inflammatory diseases, like rheumatoid arthritis (RA) have been described to cause central nervous system (CNS) activation. Less is known about environmental factors that enable the CNS to suppress peripheral inflammation in RA. Here, we identified gut microbiota-derived histamine as such factor. We show that low levels of histamine activate the enteric nervous system, increase inhibitory neurotransmitter concentrations in the spinal cord and restore homeostatic microglia, thereby reducing inflammation in the joints. Selective histamine 3 receptor (H3R) signaling in the intestine is critical for this effect, as systemic and intrathecal application did not show effects. Microglia depletion or pharmacological silencing of local nerve fibers impaired oral H3R agonist-induced pro-resolving effects on arthritis. Moreover, therapeutic supplementation of the short-chain fatty acid (SCFA) propionate identified one way to expand local intestinal histamine concentrations in mice and humans. Thus, we define a gut-CNS-joint axis pathway where microbiota-derived histamine initiates the resolution of arthritis via the CNS.

Introduction

Rheumatoid arthritis (RA) is one of the most common and severe chronic inflammatory diseases with a lack of spontaneous resolution, which generally requires lifelong treatment with anti-rheumatic drugs. The disease is characterized by chronic synovial inflammation that leads to the destruction of the affected joints and increases disability (1). One essential step to initiate the resolution of arthritis is to prevent the influx of new cells via trans-endothelial migration from blood vessels into the inflamed synovium while at the same time draining pro-inflammatory cells leave the affected joints. Earlier studies showed the potential impact of the central nervous system (CNS) and sympathetic nerve fibers in control of blood flow and vascular permeability in the arthritic joints (2, 3) and its direct relevance for resolution (4, 5). However, little effort has been made to unravel how these processes are controlled and whether and how environmental factors, such as the microbiota, can initiate resolution of arthritis via the CNS. That is surprising given the vast literature on microbial dysbiosis (6, 7), the mucosal origin hypothesis (8), or the gut-joint axis (9) and its substantial role in RA.

Beyond joint pathology, RA is associated with neuropsychiatric comorbidity including depression (10), anxiety (11), and an increased risk of developing neurodegenerative diseases in later life (12). However, the potential contribution of chronic pain to the development of depression and anxiety should not be overlooked. Pre-clinical studies from the early 90s (13, 14), and 2000s (15-17) highlighted the potential neuro-immune crosstalk in animal models for RA by showing that peripheral synovial inflammation is closely linked to the CNS.

In the CNS, the biogenic vasoactive amine histamine, which is known for its acute immediate hypersensitivity responses, also acts as a neurotransmitter in the histaminergic system. Histamine was shown to have pleiotropic effects on immune cells that are dependent on signalling via one of its four receptors (H1R-H4R). In preclinical models of arthritis, cellular-derived histamine was so far described to exert pro-arthritic effects (18) mainly via H4R expression on hematopoietic cells (19, 20) and by stimulating osteoclastogenesis (21). In

111 contrast, H3R is expressed by cells of the CNS and histaminergic neurons but also on intestinal
112 endocrine cells (22) such as enterochromaffin cells (23) linking the gut to the CNS (24). Recent
113 studies using human H3R ligands revealed anti-inflammatory effects of H3R activation on
114 neuroinflammation (25), matching reports of exacerbated neuroinflammatory disease in H3R
115 knockout mice (26).
116 In addition to mammalian cells, bacteria can also secrete histamine following decarboxylation
117 of histidine via the enzyme histidine decarboxylase (HDC) (27). However, the influence of
118 microbiota-derived histamine on host immunological processes, i.e. the resolution of
119 inflammation is yet poorly understood (28).
120 Here, we exploited untargeted metabolomics and mRNA sequencing of microglia from spinal
121 cord tissues after oral histamine treatment in collagen-induced arthritis (CIA) or experimental
122 autoimmune encephalomyelitis (EAE) mice to identify potential pro-resolving mediators of
123 synovial and central inflammation; assessed their function in vivo using PLX-5622-driven
124 microglia or QX-314 + bupivacaine-induced nerve fiber blockage; and extended these findings
125 to functional magnetic resonance tomography (MRT) analysis for vascular permeability in
126 synovial tissues. The resulting data emphasizes the importance of an acutely induced
127 inflammatory microglial phenotype for arthritis persistence, which can be restored to a
128 homeostatic microglial gene expression profile by microbiota-derived histamine, resulting in
129 rapid resolution of synovial inflammation.
130 Taken together, these data highly contribute to our understanding of the gut-joint axis by
131 implicating CNS microglial cells as a direct mediator of inter-organ signaling, thereby
132 providing alternative therapeutic options to resolve arthritis. Further, fiber-rich or short-chain
133 fatty acid (SCFA) propionate treatments naturally increased microbiota-derived histamine
134 levels in mice as well as RA and multiple sclerosis (MS) patients. These are important findings
135 as they imply the value of minimally invasive treatments, such as diet and supplementation in
136 resolution of inflammation.

Results

Propionate-induced microbial metabolites transfer pro-resolving effects

Prophylactic nutritional fiber or propionate supplementation was shown effective in RA and MS animal models (29, 30). To study potential therapeutic effects, we supplemented the drinking water of CIA mice from the peak of disease at 30 days past infection (dpi) with 150mM propionate (C3) or high fiber supplementation. Twenty days following C3 or high fiber supplementation CIA mice showed significantly improved clinical signs of arthritis (Figure 1A and Supplemental Figure 1A-C), reduced splenic Th17 cells (Figure 1B and Supplemental Figure 1D), and restored systemic bone density compared to respective non-treated controls (Figure 1C). C3 treatment increased total SCFA concentrations in the intestine (Figure 1D) and reestablished a gut microbial composition similar to the pre-clinical phase in healthy controls by reducing previously identified arthritis-related species such as from the *Akkermansiaceae (31)* and *Enterobacteriaceae (32)* family while increasing the Shannon index over non-C3-treated-CIA control mice. (Figure 1E and F). To address whether C3-modulated microbiota contributes to this finding, we established a fecal microbiota (FM) transfer model in CIA mice (Figure 1G). To that end, FM donor DBA/1 mice were supplemented with C3 in the drinking water for 3 weeks. FM (C3 FM) was harvested and further divided into FM pellet (C3 pellet) and FM supernatant (C3 supernatant) following centrifugation. Similar to therapeutic C3 supplementation in the drinking water, C3 FM transfer, when done at the peak of arthritis, promoted fast resolution compared to transfer of control FM (Figure 1H). Comparing the efficacy of the two treatments from the peak of the disease, the administration of C3 FM leads to a significant improvement in arthritis scores after only 5 days, while the supplementation of C3 in drinking water only leads to a significant improvement after 20 days. Within the three FM transfer groups, only C3 supernatant was as effective as complete C3 FM, while the C3 pellet fraction showed no statistical clinical improvement (Figure 1H). This finding was reflected in the flow cytometry analyses of spleen cells, which showed that splenic Th17 cells

decreased fast after C3 FM treatment as well as after supplementation of C3 in the drinking water (Supplemental Figure 1E). Comparison of 16S rRNA bacterial community profiles following C3 FM transfer revealed clear differences in the β-diversity 5 days after transfer over FM controls (Figure 1I) and an enrichment in *Lactobacillaceae* accompanied by lower levels of *Lachnospiraceae* (Figure 1J and K). 16S rRNA analysis revealed further enriched *Lactobacillaceae* in C3 supernatant over C3 pellet group (Supplemental Figure 1F). The effectiveness of *Lactobacillaceae* as probiotics, especially for *Lactobacillus johnsonii*, which was increased in our experiments, has been shown in a variety of inflammatory diseases (33-35).

Because C3 supernatant FM transfer was equally effective as complete C3 FM, we next performed untargeted metabolic analyses to identify possible effector molecules induced by C3 nutritional supplementation. Volcano plots of C3 supernatant FM identified significant up-, and downregulated metabolites over FM control supernatant (Figure 1L). Next, to identify responsible effector molecules in C3 supernatant FM, size exclusion chromatography (SEC) was used to separate the supernatant into 5 sub-fractions with different ranges of molecular size. Strikingly, only C3 supernatant FM fraction number 1, containing only the smallest molecules, showed similar pro-resolving effects as unfractionated C3 supernatant FM (Supplemental Figure 1G and H). Untargeted metabolomics analysis of the non-fractioned C3 supernatant identified histamine among the most upregulated metabolites, which is also part of the pro-resolving Fraction 1, due to its small molecular weight of 111.15 Dalton (Figure 1K). Another report also showed a tendency for histamine levels to increase in the colon after C3 treatment (36). Together, all these observations suggest potent peripheral pro-resolving effector functions of intestinal histamine that is locally increased in the intestine following high fiber or C3 dietary supplementation in mice.

Resolution of arthritis depends on intestinal histamine and H3R signaling

We then attempted to identify the metabolite responsible for that prompt pro-resolving effect to continue with targeted mechanistic analyses. Therefore, CIA mice (30 dpi) were orally treated with histamine at concentrations as identified in histamine ELISA of stool extracts from the MS and RA patient samples (175.2nM ± 210.8) (Supplemental Figure 2A). Oral treatment with 125 nM histamine at the peak of disease rapidly improved clinical arthritis scores in CIA mice within 5 days of treatment (Figure 2A). Histological analysis of hind paws confirmed this observation showing reduced inflammatory lesions in the joints of histamine-treated CIA mice (Figure 2B). Multiplex cytokine and chemokine immunoassays of respective sera revealed specifically differences in CCL5 and CCL2 immune cell chemotactic cytokines, whereas other mediators remained unchanged (Figure 2C and Supplemental Figure 2B-S). Further, β-diversity analysis together with taxonomic profiling of the bacterial community following 16S rRNA amplicon sequencing identified changed intestinal microbiota compositions following oral histamine treatment, again with an increased relative abundance of *Lactobacillaceae* (37) (Figure 2D-F). Furthermore, members of this family, such as *Lactobacillus reuterii* have been described as histamine producers in the intestine. Histamine produced by *Lactobacillus* inhibited proinflammatory cytokine production (38). This led us to investigate if microbial-secreted histamine would have similar pro-resolving effects as orally supplemented histamine on synovial inflammation. Recently, Barcik et al. (39) developed an *Escherichia coli* BL21 (*E.coli*) strain that was genetically modified to express the *Morganella morganii* derived histidine decarboxylase enzyme (HDC) (*E.coli* HDC^+), which is responsible for catalyzing the decarboxylation of histidine to histamine. Oral transfer of *E.coli* HDC^+ at the peak of disease significantly reduced arthritis in CIA mice compared to *E.coli*-treated or untreated CIA control mice (Figure 2G and Supplemental Figure 2T-V).

Histamine was shown to exert its effects via four different histamine receptors H1R-H4R (40). These receptors differ in their affinity for histamine, with H1R and H2R having a lower affinity

and H3R and H4R having a higher affinity (41). Oral treatment of CIA mice with selective H1R-H4R agonists at peak of disease (30 dpi) identified that only the H3R agonist replicated the strong pro-resolving effects of histamine itself (Figure 2H). This pro-resolving effect was independent from the type of H3R agonist used, as both R(-)-alpha-methylhistamine dihydrochloride (RαMH) (42) and Immethridine dihydrobromid (IDHB) (43) showed similar pro-resolving effects (Supplemental Figure 3A). To confirm that only a site-specific increase of histamine in the intestine is initiating the resolution of arthritis, we compared intraperitoneal (i.p.) and intrathecal (i.th.) to oral treatment with H3R agonist in CIA mice (Supplemental Figure 3A, B). Only oral delivery showed significant pro-resolving effects on arthritis along with increased intestinal length (Supplemental Figure 3C), as an indicator for reduced intestinal inflammation. Moreover, with increasing H3R agonist concentrations, pro-resolving effects disappeared and even exacerbated clinical arthritis scores were observed (Supplemental Figure 3D). While t-distributed stochastic neighbor embedding (t-SNE) plots of flow cytometry analysis in spleen did not show differences in cell clustering with H3R agonist treatment (Figure 2I), $CD4^+$ T cells and Th17 cells decreased in the synovial tissue (Figure 2J and K) and Th17 cells, neutrophils and $CD8^+$ T cells decreased in the draining popliteal lymph node (pLN) after H3R agonist treatment (Figure 2L-N). As previously shown by others and us, a key mechanistic contributor to the anti-inflammatory effect of C3 is the induction of regulatory T cells (Treg) (44, 30). However, H3R agonist treatment does not induce regulatory T cells (Supplemental Figure 3E). Therefore, the pro-resolving mechanism of C3-induced intestinal histamine is independent of the classical C3-associated Treg induction. Together, these results demonstrated low-level histamine concentrations in the intestine promote the resolution of arthritis via local H3R signaling.

H3R agonist stimulates the enteric neural system in arthritic mice causing anti-inflammatory responses

Our results show, that low dosage bacteria-derived histamine induces resolution of inflammation via specific H3R activation in the intestinal tract. H3R is mostly expressed on cells of the nervous system. In the intestine specifically, expression is interestingly limited to cells of the enteric nervous system (ENS) (45) and a very low number of endocrine cells (22). To assess H3R induced changes in the ENS, we applied an ex vivo gut organ culture system (46) that maintains tissue architecture, yet allows tight experimental control to perform whole-mount staining on the myenteric plexus after H3R agonist stimulation (Figure 3A). The *c-fos* gene is induced by a broad range of stimuli, and has been commonly used as a reliable marker for neuronal activity (47). Histological mean fluorescence intensity (MFI) quantification in wildtype ex vivo gut organ cultures following H3R agonist (RαMH) treatment revealed increased *cFOS* nuclear localization in βIII-Tubulin (*Tuj1*)-positive myenteric neurons (Figure 3B), consistent with previously published results by Breunig et al showing increased excitation of enteric neurons through H3R activation (48).

Bulk RNAseq experimental data from intestinal tissues of in vivo H3R agonist (RαMH) treated CIA mice revealed significant differences in gene expression profiles over non-treated CIA mice (Figure 3C). Gene ontology analysis showed that oral H3R agonist treatment of CIA mice induced a prominent inflammation suppressing phenotype in the intestinal tissue (Figure 3D). The most suppressed genes were associated with adaptive immune response (*CD3g*, *Jchain*, *Btla*, *Tnfrsf17*), lymphocyte mediated immunity (*Iglc2*) and B cell mediated immunity (*IL7R*, *Igha*) (Supplemental Figure 4). These findings were further supported by untargeted metabolomics analysis of serum metabolites (Figure 3E). Metabolites, which were increased upon H3R stimulation, were uridine and 3-Hydroxybutyric acid, which are not only known for their anti-inflammatory properties (49, 50) but also for their role in neuroprotection (51, 52) and suppression of microglia responses (53). Taken together these data suggest, that local H3R

activation in the intestine induces an anti-inflammatory milieu, and increases the neuronal activity of enteric neurons.

Microglia depletion impairs pro-resolving effects of histamine

To formally address the contribution of the central nervous system in histamine-mediated resolution of arthritis, we next characterized cellular changes in the CNS followed by respective in vivo cell depletion assays. Peripheral inflammation increases *p38* phosphorylation in neurons and microglia, especially in the dorsal horn in the spinal cord (54, 55) . As demonstrated by Boyle et al., local inhibition of p38 phosphorylation in the spinal cord did suppress arthritis(15). Analysis of the lumbar area (L3-L6) of the spinal cord (Figure 4A) that innervates the paws (56), following oral H3R agonist treatment in CIA mice showed reduced *c-fos* and *p38* phosphorylation (Figure 4B and C). Spectral flow cytometry multiparameter analysis of spinal cord single cells revealed significant cellular changes following H3R agonist treatment in CIA mice (Figure 4D), most prominent within the $CD86^+$ microglial cell fraction that was restored to the levels observed in healthy control (HC) mice (Figure 4E). Further microglial characterization revealed a shift from inflammatory back to $TMEM119^+$ homeostatic microglia (Figure 4F). Interestingly, when we treated microglia, astrocytes or neurons directly with H3R agonist in vitro, we could not observe lower levels of inflammatory gene expression or of CCL2 and CCL5 chemokine secretion (Supplemental Figure 5). When applying oral H3R agonist treatment around peak disease in the EAE animal model for MS, where microglial cells were shown to promote inflammation (57, 58), we significantly attenuated clinical scores and reduced inflammatory microglial cells in the spinal cord (Supplemental Figure 6) as seen in CIA mice. Next, we investigated the influence of microglia in CIA mice using the colony stimulating factor 1 receptor inhibitor, PLX5622 (PLX), to deplete the microglia population (58-60). Effective depletion was confirmed 3 days after last PLX treatment in CIA mice (Supplemental Figure 6G). Following short-term PLX treatment (25–30 dpi) in CIA mice, the

prominent H3R agonist-mediated pro-resolving effects were lost when microglia were depleted (Figure 4G). Taken together, these results show that H3R activation in the intestine results in a phenotypic switch from pro-inflammatory to homeostatic microglial cells in the spinal cord, which are essential for the H3R induced resolution of arthritis.

Oral H3R agonist treatment influences microglia function in the spinal cord

Our finding that microglia are essential for the intestinal histamine-induced resolution of arthritis prompted us to analyze their transcriptomes in CIA mice following oral H3R agonist treatment. Therefore, $CD11b^+$ spinal cord microglia were isolated from CIA mice after oral H3R treatment and processed for bulk RNA sequencing (Figure 5A and Supplemental Figure 6H). Microglia from H3R agonist treated CIA mice showed a significantly altered gene expression profile, predominantly characterized by an increase of immune modulatory genes such as *Fmr1nb, C4b, Spp1* and *CD72* (61-64) (Figure 5B). Gene set enrichment analysis (GSEA) of hallmark genes revealed an overall anti-inflammatory phenotype. Inflammatory pathways such as IL-6, JAK/STAT3 and TNFα signaling were downregulated whereas anti-inflammatory pathways such as oxidative phosphorylation were upregulated (Figure 5C). Further, analysis of the microglial microenvironment by untargeted metabolomics in spinal cords of H3R treated CIA mice identified a significantly changed secreted metabolite pattern with increased thiamine, acetylcholine and gamma-aminobutyric acid (GABA) in lumbar spinal cord tissue supernatants (Figure 5D). Of note, identical spinal cord metabolites were previously linked to attenuated clinical scores in RA (65, 66) by reducing *p38* phosphorylation in the CNS (15, 67). Metabolite set enrichment analysis (MSEA) of identified spinal cord metabolites revealed the aspartate and purine metabolism as well as arginine biosynthesis amongst the highest enriched metabolites (Figure 5E). L-arginine was previously shown to inhibit arthritis and associated inflammatory bone loss in mice (68). In addition, RA patients exhibit lower purine metabolism activity (69), and a shortage of aspartate was shown to fuel synovial

inflammation in RA (70). Together, these data identify oral histamine as a pro-resolving regulator of microglial gene expression and spinal cord metabolites.

Intestinal H3R signaling reduces vascular leakage in inflamed paws

Microglia sense neuronal activity and can directly modulate their functions (71). In RA models, sciatic nerve branches were shown to control vascular leakage in arthritic paws (72-74). Therefore, plantar nerve fibers were isolated from the peak of activity of CIA following oral H3R agonist treatment. Sort-purified $CD11b^-$ nerve cells were analyzed by bulk RNAseq (Figure 6A). The genes most differentially expressed included representatives of several signaling pathways critical for regulating cell and tight junction organization as well as GABA receptor activation and neurovascular coupling as indicated by enriched pathway analysis (Figure 6B). Further analysis of upstream regulators for neurovascular coupling signaling identified nuclear receptor (NR) *Nr4a3* and *Mef2c* as most significantly upregulated, both described to be involved in vascular biology and microglial inflammatory responses (75, 76) (Figure 6C, Supplemental Figure 7A and B). The Smoothelin-Like Protein 1 (SMTNL1) upstream regulator was most reduced in plantar nerve $CD11b^-$ cells, similar to what was found in K/BxN mice following denervation of the sciatic nerve (74) (Figure 6C).

To analyze actual changes in vasoconstriction and vasodilation in CIA paws, in vivo magnetic resonance imaging (MRI) was performed at 28 and 31 dpi, before and after oral H3R agonist treatment, respectively. Reduced K_{ep} values, indicative of reduced vascular leakage, were found in H3R agonist-treated mice (Figure 6D) along with overall lower raw signal intensity after contrast agent application (Figure 6E and F). Furthermore, the tendency to lower inflammatory area and paw thickness could be identified by MRT as soon as the last H3R agonist intervention administration (Supplemental Figure 7C and D). Also, a reduction of synovial $CD4^+$ T cells was visible 8 days after the last RαMH treatment (Supplemental Figure 7E). To investigate the dependence between the microglia changes in the spinal cord and the vascular leakage in the

joints, we used a pharmacological approach to temporarily shut down nerve activity (73). QX-314, a membrane-impermeable lidocaine derivative that must enter a cell to block sodium channel conductance was locally injected in combination with bupivacaine in the footpad minutes before H3RA treatment at peak activity days of CIA. QX-314 treatment did not directly affect paw thickness in CIA mice, but abrogated the anti-inflammatory effects following oral H3R agonist administration (Figure 6G). Together, this data suggest that local intestinal H3R activation restores vascular leakage in the inflamed joints by affecting centrally controlled local nerve innervation.

Propionate supplementation increases local histamine levels in RA and MS patients

To translate our findings to human disease we utilized samples from two human studies, where RA and MS patients were supplemented with the SCFA propionate over the time course of several weeks. In the "ProDarMi" study (German Clinical Trials Register ID: DRKS00023985) healthy subjects were compared to patients with RA, RA-at risk, psoriatic arthritis, psoriasis or ankylosing spondylitis (AS). The publication of the initial clinical studies showed the beneficial effect of C3 or high fiber supplementation on disease activity of the patients (77-80). To elucidate if this effect of propionate is due to an increase in local histamine levels in the gut in the human setting, we analyzed stool samples from these patients at baseline and after 28 days (RA patients) or 90 days (MS patients) of C3 treatment. Interestingly, C3 supplementation over the course of 28 and 90 days significantly increased histamine levels in the stool samples of the patients (Figure 7A and B). To further elucidate the role of microbiota-derived histamine we reanalyzed RNAseq data from the ex vivo gut explant model utilized by Duscha et al (77), where the gut explants were treated with the microbiota of patients before and after C3 supplementation. Here, we looked at genes that are associated with H1R and H2R activation. Interestingly, H1R and H2R associated genes (histamine response network) were downregulated after C3 treatment (Figure 7C), although local histamine levels were

significantly increased. This observation supports our hypothesis that this low-level histamine derived from microbiota acts via H3R activation and does not induce allergy or intolerance-associated reactions, mediated by H1R or H2R activation. Furthermore, histological analysis of H3R expression in ileal biopsies of RA patients and healthy controls revealed low levels of H3R expression in the healthy controls, consistent with previously published data (45). In RA patients, however, H3R expression in ileal tissues was strongly increased (Figure 7D and E). To further strengthen the translational aspect of our manuscript, we had the unique opportunity to retrospectively analyze fecal microbiota transfer (FMT) samples from the published FLORA trial (clinical trial number NCT03058900, (81)) within an ongoing collaboration. Our analysis revealed that FMT recipients who received stool samples with high histamine concentrations showed a 100% improvement in clinical response in a small sample group (Figure 7F). Furthermore, we found significant differences in fecal histamine concentrations among FMT recipients, with higher histamine levels associated with clinical improvement (Figure 7G). Taken together, these data indicate that our results in preclinical models may be applicable to human patients.

Discussion

The concept that the nervous system senses environmental stimuli and transmits these signals to immune cells to maintain tissue homeostasis is well-established (82). However, during chronic arthritic inflammation, it has been shown that the nervous system can exert both, pro-inflammatory or anti-inflammatory functions. For example, non-invasive electrical vagus nerve stimulation was shown effective to attenuate arthritis in CIA mice and RA patients (83, 84). On the other hand, denervation of the sciatic nerve protected mice from K/BxN serum transfer arthritis and individuals who suffer paralysis on one side of the body developed arthritis only on the neurologically unaffected contralateral side (74, 85).

So far, irrespective of the clinical effects, the regulation of arthritis by the CNS has only been investigated in a two-dimensional approach between the CNS and the joints. Here we identified spinal cord microglia as an essential gut-joint interface responsible for transmitting the anti-inflammatory pro-resolving effect of microbiota-derived histamine to the joints, thereby extending the neuro-immunomodulatory concept in RA to a third dimension, the gut.

Building on seminal work from both the Firestein (15-17) and Straub (86-88) publications who postulated the CNS as a potential target for the treatment of rheumatic diseases, we experimentally confirmed their previous observations of reduced c-Fos protein expression and p38 phosphorylation locally in the spinal cord after i.th. application of p38 or TNFα inhibitors, simply by oral histamine supplementation. That is relevant because peripheral inflammation increases the percentage of neurons with p38 activation in the spinal cords of mice (89).

By involving higher structures of the brainstem, the CNS effectively controls systemic immune responses broadly via the hypothalamic-pituitary axis (HPA) and the release of anti-inflammatory glucocorticoids by the adrenal cortex. These effects stand in contrast to the somatic sensory afferent fibres in the arthritic paws, which are under the local control of the spinal cord and send signals back to the periphery through so-called antidromic action potentials of the dorsal root reflex (DRR) (90, 91). This reflex is mainly pro-inflammatory through the

recruitment of inflammatory cells and by promoting vasodilation and vessel leakiness as somatic denervation in mice was shown to protect from inflammatory arthritis (91). We could show by in vivo magnetic resonance imaging (MRI) that shortly after oral H3R agonist treatment vessel leakiness in the inflamed paws of CIA mice was likewise reduced and by temporarily shutting down nerve activity, the pro-resolving effect of histamine was lost.

The autonomic nervous system is part of the CNS that regulates involuntary body functions and is considered essential for the control of the regional homeostasis at the level of individual organs. The autonomic nervous system comprises two main branches: the sympathetic and parasympathetic. Parasympathetic stimulation was shown to suppress peripheral activation via the so-called cholinergic reflex that is triggered by the major parasympathetic neurotransmitter acetylcholine (ACh) (92, 93). Interestingly, ACh was among the most upregulated metabolites identified in spinal cord tissues following oral H3R agonist treatment in the current study, which is in accordance with previous reports showing H3R-dependent ACh release by histaminergic neurons (94). In preclinical RA models, ACh that was shown to effectively attenuate arthritis and genetic knockdown of the alpha7 nicotinic acetylcholine receptor (α7nAChR) increased CIA severity in mice (17, 66, 95, 96).

Next to ACh, we found GABA as significantly increased in spinal cord tissues following oral H3R treatment. GABA is a non-proteinogenic amino acid that is widely present in microorganisms, plants, and vertebrates and known to act as an inhibitory neurotransmitter in the CNS. Cadherin-13 (CDH13) was shown to be a critical regulator of GABAergic modulation (97) and was found upregulated amongst most significant genes in sort purified microglia following oral H3R agonist treatment. GABA agonist treatment effectively improved clinical signs in a rat model of chronic inflammatory pain (98). The role of GABA signalling in arthritis has also been investigated showing that the GABAergic system counteracting both the development and progression of RA (99), potentially by dampening T- and antigen-presenting cells (APC) activity (100). Notwithstanding the fact that GABA levels have been shown to be

lower in people with RA compared to healthy individuals (101), the role of the GABAergic system in RA is complex and further research is needed to unravel its functions.

Acute peripheral inflammation was shown to increase glutamate in the spinal cord (102) as seen in the spinal cords of CIA mice following H3R agonist treatment. Glutamate, together with ACh and GABA, was described as potent modulator of the microglia phenotype, shifting them to an anti-inflammatory homeostatic phenotype (103, 104) that we mimic with the microglia phenotype after H3R agonist treatment. As shown by two independent studies on CIA-, or *TNFa*-transgenic arthritis mouse models and on post-mortem brain tissue from people with RA, microglia per se exhibit an inflammatory transcriptomic phenotype during active disease (105, 106). We identified myocyte-specific enhancer factor 2C (MEF2C) as strongest induced upstream regulator in sorted nerve cells following H3R agonist treatment and MEF2C was shown to restrain microglial inflammatory response (75). Pharmacological silencing of primary afferents in arthritic joints prevented microglial activation (73) and depletion of activated microglia in the EAE model delayed disease onset while microglia-specific deletion of the non-canonical NF-kappaB-inducing kinase (NIK) impaired EAE disease progression (57, 58). The increase in homeostatic microglia in the CIA+RαMH group compared to the CIA group is highly relevant to the resolution of inflammation and represents a key focus of our study. Notably, we also observed this increase in the CIA+RαMH group relative to HC control mice, which is a to our understanding novel and intriguing finding that warrants further investigation. This observation may have important implications for the development of prophylactic strategies aimed at enhancing homeostatic microglia during the early stages of disease, potentially mitigating the expansion of inflammatory microglia. Together with published data, our findings suggest a central role for microglia in the gut-specific H3R signalling-mediated resolution of inflammation.

A limitation of this study is that the main conclusions regarding the central role of microglia are based on microglial elimination using PLX5622. Our data show that in CIA mice, short-

term PLX treatment led to the loss of the pronounced pro-resolving effects mediated by the H3R agonist. We used PLX5622 to assess the dependence of these effects on microglia, assuming that its action was restricted to microglia. However, recent evidence suggests that PLX5622 also affects myeloid compartments in the bone marrow and spleen (107). It is important to note that the treatment regimens in this study differ fundamentally from our approach in terms of duration and intensity. Future studies should employ microglia-specific genetic models to refine our findings. Currently, a major limitation of existing genetic microglia depletion models for our study is twofold: first, their often-low specificity, and second, the C57BL/6 genetic background of these strains, which renders them resistant to the CIA model used in our study. In addition, it would be helpful if the number of cells per mg of tissue were also given in the following investigations in order to be able to better estimate the total number of infiltrating cells in the synovium or in the LN or to determine whether only a lower percentage of certain cell subsets are present. Furthermore, our dose-dependent results indicate that the loss of pro-resolving effects and the worsening of arthritis scores at higher H3R agonist concentrations suggest that establishing an effective dosage may be challenging when translating these findings to human disease.

We propose that microbiota-derived histamine in the gut stimulates the enteric nervous system via H3R signalling (48). This tissue-specific response to histamine triggered the restoration of anti-inflammatory homeostatic microglia in the spinal cord where pro-inflammatory microglia were found to be enriched during pre-clinical arthritic models and RA patients (105, 106). Both the transcription profiles of the microglia and the secreted metabolites in the spinal cord create a local anti-inflammatory environment that causes a reduction in vasodilation and an egress of inflammatory cells from arthritic paws via efferent nerve fibres. We also found that disrupting this gut-CNS-joint axis either by depleting microglia in the spinal cord or by blocking nerve fibres in the paws abolished the pro-resolving effect of histamine. In addition, high-fibre diet

499 or direct SCFA-propionate supplementation increases local histamine concentrations in the gut
500 of RA and MS patients thereby supporting resolution of inflammation.
501

Methods

Sex as a biological variable

For all experiments female mice were used, because of their higher susceptibility to CIA. This aligns with human RA, which is more prevalent in women.

Mice

Five- to six-week-old WT C57BL/6N (Charles River) and DBA/1J mice (Janvier) were acclimated for 1 week, followed by a 3-week co-housing period before starting the experiments. All mice were maintained under specific pathogen-free conditions at the Präklinisches Experimentelles Tierzentrum (PETZ) Erlangen, Germany. Supplementation of sodium propionate (Sigma-Aldrich) was done in the drinking water at a final concentration of 150 mM and changed every 3 days. The animals received water w/wo C3 and standard chow (Ssniff Spezialdiäten GmbH) ad libitum.

Human studies

Demographic characteristics of RA C3 supplementation study: Age, mean ± SD, years = 49,46 ± 14,88; Females, N (%) = 12 (85,71%); Disease-specific characteristics: Disease activity score (DAS) 28 ESR, mean ± SD, units = 3,1 ± 1,48; DAS 28 CRP, mean ± SD, units = 2,71 ± 1,49). Demographic characteristics of the MS study: Age, mean ± SD, years = 51,32 ± 13; Females, N (%) = 12 (42,86%).

Flora trial: FMT Donors were between 25 - 55 years old. Demographic characteristics of FMT patients: Age, mean ± SD, years = 48,9 ± 16,1; Females, N (%) = 8 (53%).

Collagen-induced arthritis (CIA)

CIA was induced in 8-week-old female DBA/1J mice by subcutaneous injection at the base of the tail with 100 µl of 0.25 mg chicken type II collagen (CII; Chondrex) in complete Freund adjuvant (CFA; Difco Laboratory) containing 5 mg/ml killed *Mycobacterium tuberculosis* (H37Ra). Mice were re-challenged after 21 days intradermal immunization in the base of the tail with 100 µl of 0.25 mg chicken type II collagen (CII; Chondrex) in incomplete Freund

adjuvant. The paws were evaluated for joint swelling three times per week. Each paw was individually measured for paw thickness using a caliper or by giving an eye score using a 4-point scale: 0, normal paw; 1, minimal swelling or redness; 2, redness and swelling involving the entire forepaw; 3, redness and swelling involving the entire limp; 4, joint deformity or ankylosis or both. Mean values of paw thickness and summed eye scores were displayed.

Supplementation of Sodium Propionate in the drinking water

Mice were supplemented with 150 mM Sodium Propionate (C3, Sigma) in the drinking water. Drinking water was changed every two days to ensure consistent concentration and quality of the solution. Naïve mice were treated for 3 weeks as donors for fecal microbiota transfers (FMT), CIA mice were treated starting from peak of disease severity (30 dpi).

Fecal microbiota transfer (FMT)

Donor mice were treated for at least three weeks with 150 mM sodium propionate (C3) in the drinking water. For transfer into five recipient mice, two donor mice were sacrificed, and their cecum contents were mixed with 2.5 ml 1 x PBS (for transfer) or H20 (for FPLC or untargeted metabolomics). The mixture was filtered through a 100 µm cell strainer. Then, 250 µl of the filtered solution was transferred into the donor mice by oral gavage. To guarantee the stability of the transfer, the procedure was repeated after two days. To assess the effect of soluble components or bacterial and cellular matters on ongoing CIA in mice the stool mixture was centrifuged at 3000 g. Supernatant fraction was aspirated and pellet was resuspended in PBS before transfer into mice with CIA by oral gavage.

Culture and transfer of *E.Coli* strains

Frozen *E.Coli* glycerol stocks (kindly provided by Cezmi Akdis, Davos) were inoculated in 5 ml LB Medium (Roth). Bacteria were incubated overnight in a bacteria shaker at 37 °C, and 300 rpm. The next day the OD450nm was measured every hour until reaching the exponential phase. DBA1/J mice were treated with *E.Coli* B21 ± HDC by oral gavage. Each mouse received

553 $1x10^8$ per 250 µl dose reconstituted in PBS. Control mice received 250 µl PBS by oral gavage.
554 Treatment was performed twice at days 30 and 32 post immunization.

555 **Fraction-generation by Fast protein liquid chromatography (FPLC)**

556 Supernatant was further separated into 5 different size-specific fractions. In a first step sample
557 was centrifuged at 100.000 g for 60 min. Supernatant was transferred on a VivaSpin 6 Column
558 with a cut-off of 3 kDa and centrifuged for about 40-60 min until the remaining supernatant
559 was 250 µl. Flow-through was collected as Fraction 1 for further transfer. Remaining
560 supernatant was collected for separation into 4 further fractions by FPLC in cooperation with
561 Xiang Wei from the Molecular Neurology Department of the UK Erlangen. Fractions were
562 aliquoted and stored on -80 °C until transfer to mice. Supernatant fractions were thawed shortly
563 before transfer into mice at peak of CIA by oral gavage. Mice were treated for 5 days with 250
564 µl of the corresponding fraction or PBS as a control

565 **Oral treatment with Histamine and Histamine-receptor agonists**

566 Histamine and Histamine receptor agonists (see table 1) were dissolved in PBS to a stock-
567 concentration of 0,5 mM and stored at -20 °C. Histamine treatment concentrations were
568 carefully selected based on histamine concentrations in the stool of RA and MS patients after
569 C3 treatment. Mice at peak of CIA were treated with 250 µl Histamine (final concentration of
570 125nM), H1R-Agonist, H2R-Agonist, H4R-Agonist (900 nM) [equipotent to histamine] or
571 H3R-Agonist (60 nM) [15x more potent than histamine] by oral gavage for 3 days.

572 **Microglia depletion**

573 Microglia were depleted using the CSF1R antagonist PLX5622. Mice received daily i.p.
574 injections with 50 mg/kg PLX5622 (reconstituted in DMSO) or DMSO as control over 5 days.

575 **Blockage of primary afferents in the paws**

576 The membrane impenetrable lidocaine sodium channel blocker QX-314 (2%, Sigma, 552233)
577 was co-administered daily with bupivacaine (10 µg, Sigma, B5274) intra-plantarily in the hind

paws for three days in combination with oral H3R agonist treatment in CIA mice at peak of disease days (28 – 30 dpi).

EAE

EAE was induced in 8-12-week female C57Bl/6J mice using 150 µg of MOG35–55 (Genemed Synthesis, 110582) mixed with freshly prepared complete Freund's Adjuvant (using 20 ml Incomplete Freund's Adjuvant (BD Biosciences, #BD263910) mixed with 100 mg Myobacterium tuberculosis H37Ra (BD Biosciences, #231141)) at a ratio of 1:1 (v/v at a concentration of 5 mg/ml). All mice received two subcutaneous injections of 100 µl each of the MOG35-55/CFA mix. All mice then received a single intraperitoneal injection of 200 ng pertussis toxin (List Biological Laboratories, #180) in 200 µl of PBS. Mice received a second pertussis toxin injection at the same concentration two days after EAE induction. Mice were monitored and scored daily thereafter. EAE clinical scores were defined as follows: 0, no signs; 1, fully limp tail; 2, hindlimb weakness; 3, hindlimb paralysis; 4, forelimb paralysis; 5, moribund.

Data analysis and statistics

Statistical analyses were performed using Prism 9 software (GraphPad). Comparisons between two groups were performed using unpaired or paired, two-tailed, Student's t test. Comparisons between more than two groups were performed using one-way ANOVA and Tukey's or Dunnett's multiple comparison test. Statistical significance: * $p < 0.05$; ** $p < 0.01$; *** $p < 0.001$; **** $p < 0.0001$. Details on the statistical analysis are listed in the figure legends.

Study approval

The RA C3 supplementation study was approved by the ethics committee of the Department of Medicine at the Friedrich-Alexander University Erlangen-Nürnberg (#431_20 B). The study protocol and Trial registration can be found in the German Clinical Trials Register (ID: DRKS00023985).

The MS study was approved by the ethics committee of the Department of Medicine at the Ruhr-University Bochum (registration number 15-5351, 4493-12, 17-6235) and all study information has previously been published (77).

All experiments were approved by the local ethics authorities of the Regierung of Unterfranken, Germany (#55.2-2532-2-424, #55.2-2532-2-1674, #55.2.2-2532-2-1180).

Data availability

All relevant data are available from the authors upon reasonable request. The source data underlying Figures 1-7 and Supplementary Figures 1-7 are provided as source data file. 16S rRNA sequencing data are deposited in publicly accessible database and available under the following accession link: https://figshare.com/s/b5a827f0fb182a57b242. The supporting data values are available in the supporting data values file (XLS).

Author contributions

G.S., V.T. and M.M.Z. designed the project, interpreted results and wrote the manuscript. K.D. and M.L. performed most of the work, analysed data, edited the manuscript and made figure panels. L.E., E.S., H.D., M.H.-S., L.L., M.F., V.A., F.S., and S.L. acquired data and provided help with multiple experiments. L.A, T.R.L. and T.S. performed and analysed 16S rRNA data. H.BM, Y.R., H.R. and N.Y. performed and analysed gut explant experiments. A.G. and R.V.T. performed and analysed untargeted metabolomics experiments. J.H. performed and analysed the SCFA measurements. D.M. and F.C. performed and analysed human H3R staining. F.B. and R.B. performed spinal cord histology. M.S.K. and T.E. performed the FLORA study and provided the FMT samples. W.X. performed size exclusion chromatography. A.H. and C.A.A. provided human MS stool samples and HDC competent *E.coli* strains, respectively. T.B. performed and analysed MRT measurements. T.B. and K.S. wrote the animal licence approvals.

M.M.Z supervised the project and provided funding. All the authors revised and approved the manuscript.

Supplemental Materials

Supplemental Figures 1-7

Methods

Supplemental Table 1

Acknowledgements

We thank the Optical Imaging Center Erlangen (OICE), Erlangen, Germany for their technical help with microscopy. We thank the Core Unit Next Generation Sequencing, Erlangen, Germany for their support. We thank Dr. Z. Winter and C. Engert from the Preclinical Imaging Platform Erlangen (PIPE) for their support with the MRI. We thank Prof. Sonnewald for his support. We thank the animal facility PETZ, Erlangen, Germany for supporting this project. We thank D. Weidner for her support with the µCT analysis. We thank B. Happich and N. Berndt from the Med3 Histology Lab for their support. We thank Dr. Wirtz from the Microbiome Analysis Core Unit (MACE), Erlangen for the 16S rRNA sequencing. We thank the Med 3 Studienambulanz for their support in collecting the study samples. We thank all members of our laboratories at the Medical Clinic 3, Erlangen, Germany for their support and helpful discussion. This study received funding from the Deutsche Forschungsgemeinschaft (DFG, German Research Foundation) via DFG-RU2886-Project A01 as well as DFG-CRC1181-Project-No. B07. This study was further funded by the Interdisciplinary Center for Clinical Research, Erlangen (IZKF) (project number P144) at the Universitätsklinikum Erlangen, Germany.

Competing interest

The authors declare no competing interests.

Table 1: Used Histamine Receptor Agonists

Name	Chemical name	Company	Cat. number
Histamine 1 Receptor Agonist	2-((3-Trifluoromethyl)phenyl)histamine dimaleate	Sigma-Aldrich, St. Louis, USA	T4951-5mg
Histamine 2 Receptor Agonist	Amthamine dihydrobromide	Sigma-Aldrich, St. Louis, USA	A4730-10MG
Histamine 3 Receptor Agonist	(R)(−)-α-Methylhistamine dihydrochloride	Sigma-Aldrich, St. Louis, USA	H128-5mg
Histamine 4 Receptor Agonist	4-Methylhistamine dihydrochloride	Tocris Biotechne	2342
Histamine	Histamine ≥97%	Sigma-Aldrich, St. Louis, USA	H7125-1g

Figures

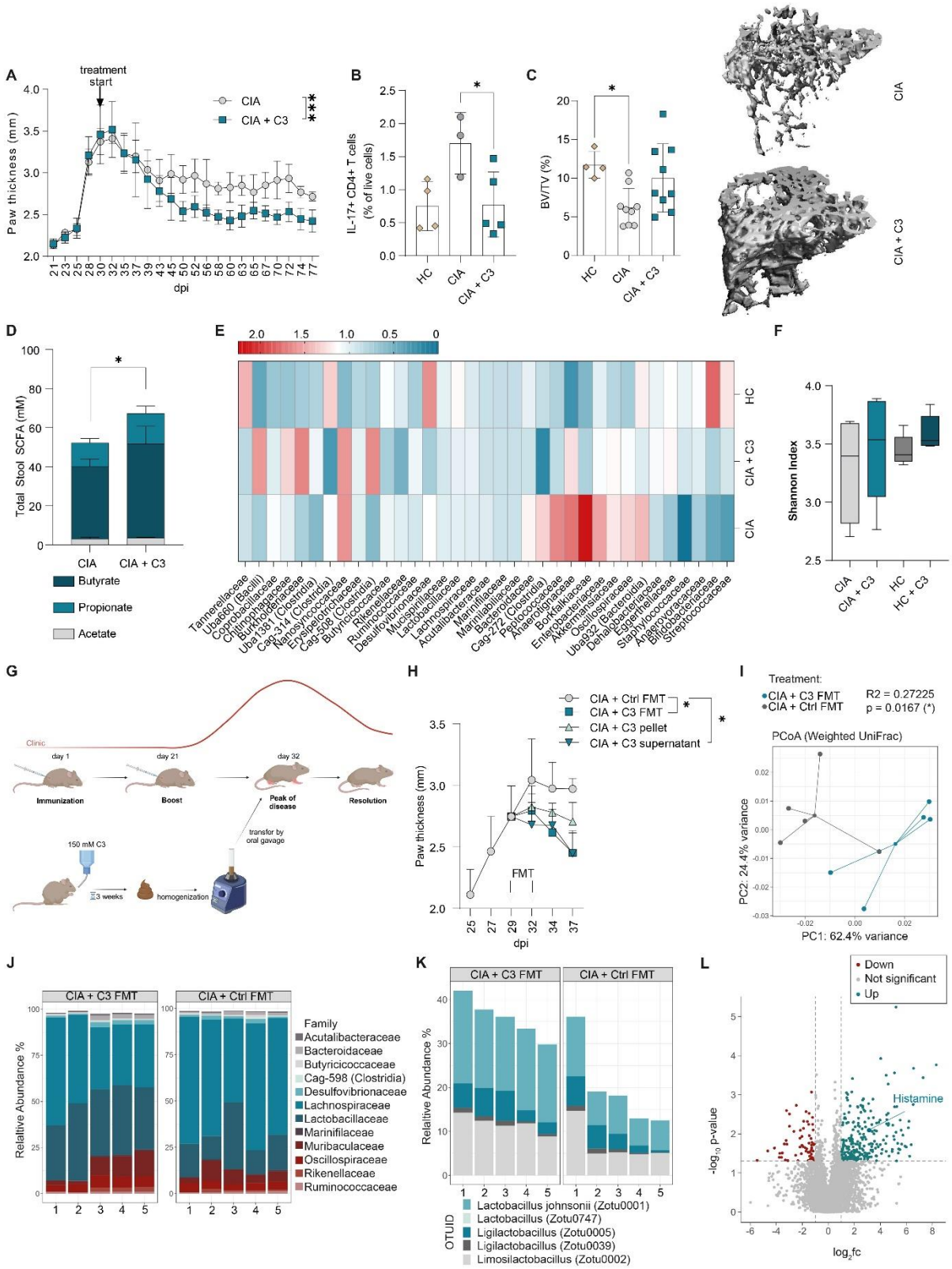
A
treatment start
CIA
CIA + C3
Paw thickness (mm)
dpi
B
IL-17+ CD4+ T cells (% of live cells)
HC
CIA
CIA + C3
C
BV/TV (%)
CIA
CIA + C3
D
Total Stool SCFA (mM)
Butyrate
Propionate
Acetate
E
HC
CIA + C3
CIA
F
Shannon Index
G
Clinic
day 1
day 21
day 32
Immunization
Boost
Peak of disease
Resolution
150 mM C3
3 weeks
homogenization
transfer by oral gavage
H
CIA + Ctrl FMT
CIA + C3 FMT
CIA + C3 pellet
CIA + C3 supernatant
Paw thickness (mm)
FMT
dpi
I
Treatment:
CIA + C3 FMT
CIA + Ctrl FMT
R2 = 0.27225
p = 0.0167 (*)
PCoA (Weighted UniFrac)
PC2: 24.4% variance
PC1: 62.4% variance
J
CIA + C3 FMT
CIA + Ctrl FMT
Relative Abundance %
Family
Acutalibacteraceae
Bacteroidaceae
Butyricicoccaceae
Cag-598 (Clostridia)
Desulfovibrionaceae
Lachnospiraceae
Lactobacillaceae
Marinifilaceae
Muribaculaceae
Oscillospiraceae
Rikenellaceae
Ruminococcaceae
K
CIA + C3 FMT
CIA + Ctrl FMT
Relative Abundance %
OTUID
Lactobacillus johnsonii (Zotu0001)
Lactobacillus (Zotu0747)
Ligilactobacillus (Zotu0005)
Ligilactobacillus (Zotu0039)
Limosilactobacillus (Zotu0002)
L
Down
Not significant
Up
Histamine
-log10 p-value
log2fc

Figure 1: Propionate-induced microbial metabolites transfer pro-resolving effects

(A) Clinical arthritis score shown as paw thickness (mm) of CIA mice ± 150 mM C3 (n=4-5) in the drinking water starting 30 dpi. **(B)** Flow cytometric analysis of IL-17+ CD4+ T cells in the spleen of healthy mice and CIA mice ± C3. **(C)** quantification of bone mass (BV/TV) and representative µCT images of the trabecular part of tibial bone of healthy mice and CIA mice ± C3, analyzed 77 dpi. **(D)** SCFA levels in the cecum content of CIA mice ± C3. **(E)** 16s rRNA sequencing of the cecum content of healthy mice, CIA mice and CIA mice ± C3 in the drinking water. **(F)** Alpha-diversity measure of 16S rRNAseq data. **(G)** Experimental layout of FMT experiment. This overview was generated with BioRender. **(H)** Clinical arthritis score shown as paw thickness (mm) of CIA mice treated with FMT of naïve donors, C3-treated donors, pellet of C3-treated donors or supernatant of C3-treated donors. **(I)** PCoA Plot of 16S rRNA sequencing of mice after control or C3 FMT. **(J)** Relative abundance of the bacterial families identified by 16S rRNA sequencing. Permutational multivariate analysis of variance (ADONIS) was significant (R2=0.27225, P = 0.0167(*)). **(K)** Relative abundance of most strongly changed *Lactobacillaceae* strains. **(L)** Volcano Plot of untargeted metabolomics analysis of stool supernatant fraction obtained from control vs C3-treated FMT donors, Cut-off were p-value < 0.05 and -1 < log2fc < 1. Data are expressed as the mean ± sd. Statistical difference was determined by ADONIS (L), One-way ANOVA (B,C,F),Student's t-test (D) and Area under the curve (A,H). *p < 0.05; **p < 0.01; ***p < 0.001; ****p < 0.0001. BV = bone volume, TV = tissue volume, CIA = collagen-induced arthritis, C3 = Propionate, dpi = days post immunization, FMT = fecal microbiota transfer.

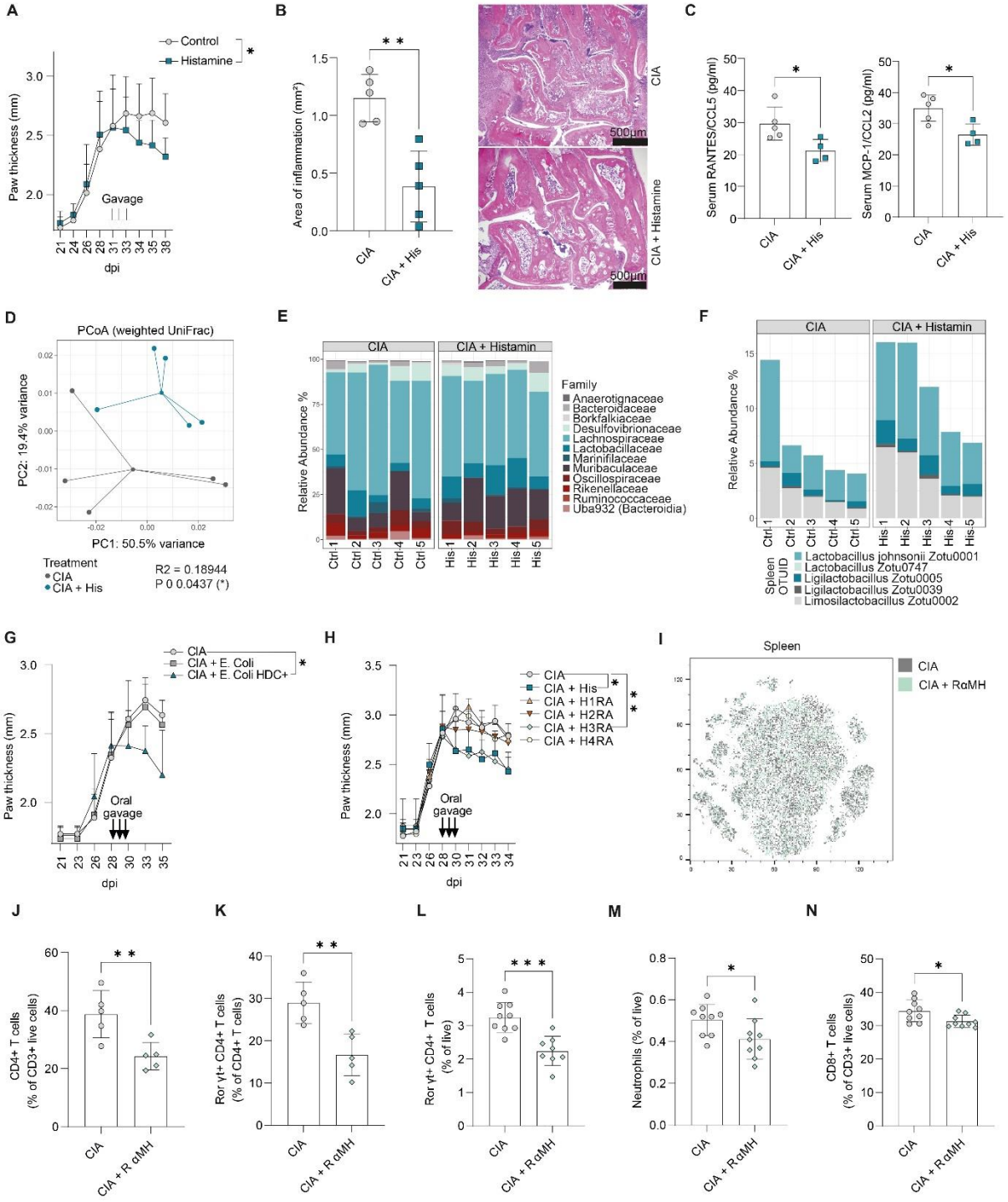

Figure 2: Resolution depends on intestinal histamine and H3R signaling

(A) Clinical arthritis score shown as paw thickness (mm) of CIA mice ± histamine (n=12-14) at peak of disease. **(B)** Area of inflammation expressed as absolute mm^2 per analyzed H&E stained paw sections of CIA mice ± histamine (n = 5) and exemplary histology pictures. **(C)** Serum levels of RANTES/CCL5 and MCP-1/CCL2. **(D)** PCoA Plot of 16S rRNA sequencing

of CIA mice ± histamine. Permutational multivariate analysis of variance (ADONIS) was significant (R2=0.18944, P =0.0437(*)). **(E)** Relative abundance of the bacterial families identified by 16S rRNA sequencing. **(F)** Relative abundance of most changed *Lactobacillaceae* strains after histamine treatment. **(G)** Clinical arthritis score shown as paw thickness (mm) of CIA mice after transfer of PBS (Control), *E.Coli* or HDC+ *E.Coli* at peak of disease (n = 4-5). **(H)** Clinical arthritis score shown as paw thickness (mm) of CIA mice after oral transfer of Histamine or specific agonists for H1R-H4R. (n = 4-5). **(I)** t-SNE Plot of spectral flow cytometric analysis of the spleen from CIA mice + H3R agonist RαMH. **(J)** CD4+ T cells in the synovium. **(K)** RORγt+ CD4+ T cells in the synovium. **(L)** RORγt+ CD4+ T cells in the pLN. **(M)** Neutrophils in the pLN. **(N)** CD8+ T cells in the pLN. Data are expressed as the mean ± sd. Statistical difference was determined by Student's t-test (B,C,J-N), t-test or one-way ANOVA of area under the curve (A,G,H), and ADONIS (D). *p < 0.05; **p < 0.01; ***p < 0.001; ****p < 0.0001. dpi = days post immunization, HR = histamine receptor, CIA = collagen-induced arthritis, pLN = popliteal lymph node.

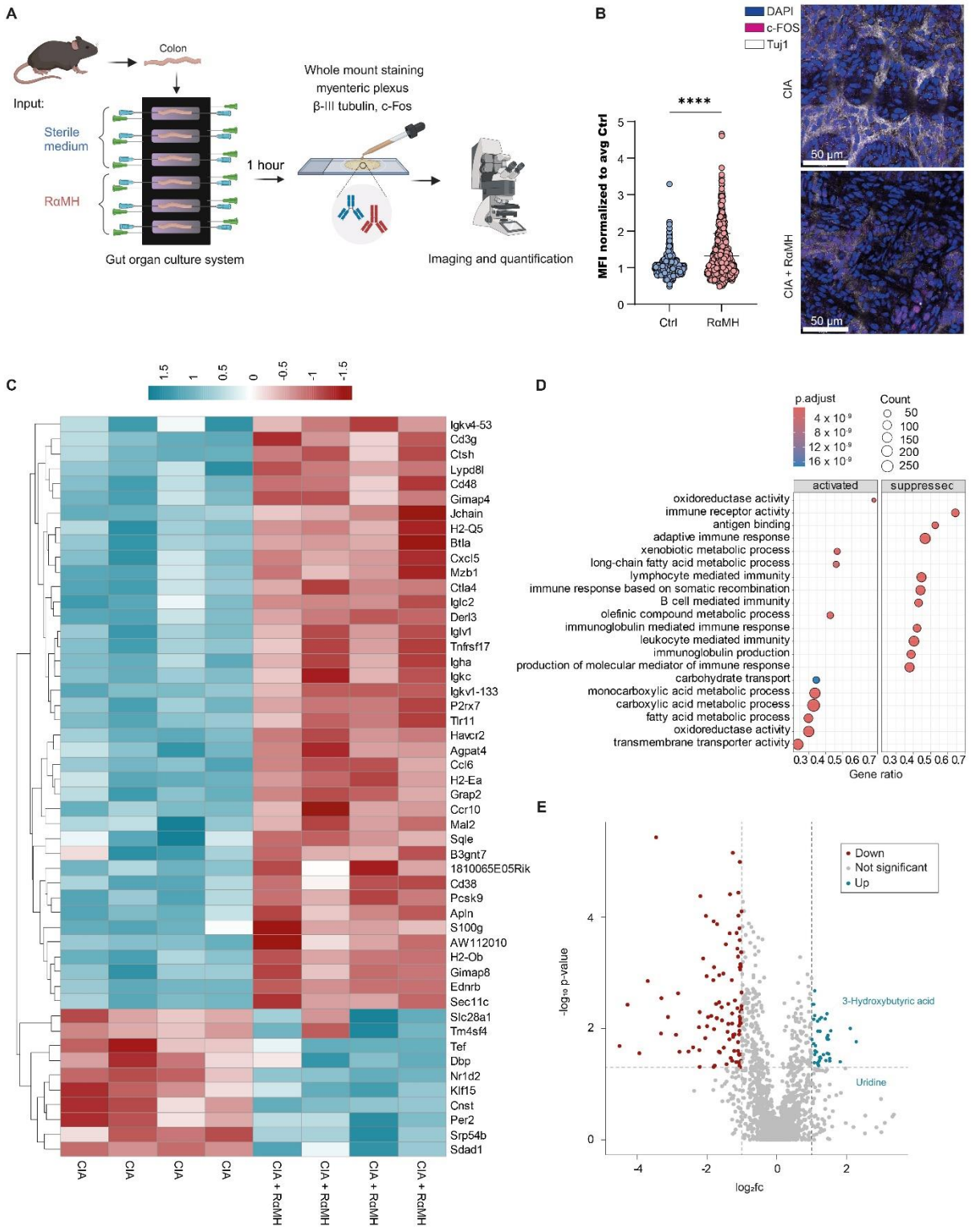

Figure 3: H3R agonist stimulates the ENS in arthritic mice causing anti-inflammatory responses

(A) Experimental layout of ex vivo intestinal organ culture system. This overview was generated with BioRender. **(B)** normalized MFI of c-FOS in βIII-Tubulin+ enteric neurons after

RαMH stimulation and exemplary pictures. **(C)** Heatmap of the top 50 regulated genes identified by RNAseq of intestinal tissue of CIA mice after in vivo RαMH treatment. **(D)** Gene set enrichment analysis (GSEA) of intestinal RNAseq data. **(E)** Volcano plot of untargeted metabolomics data of serum of CIA mice ± RαMH. Cut-off were p-value < 0.05 and -1 < log2fc < 1. Data are expressed as the mean ± sd. Statistical difference was determined by Student's t-test. ****p < 0.0001.

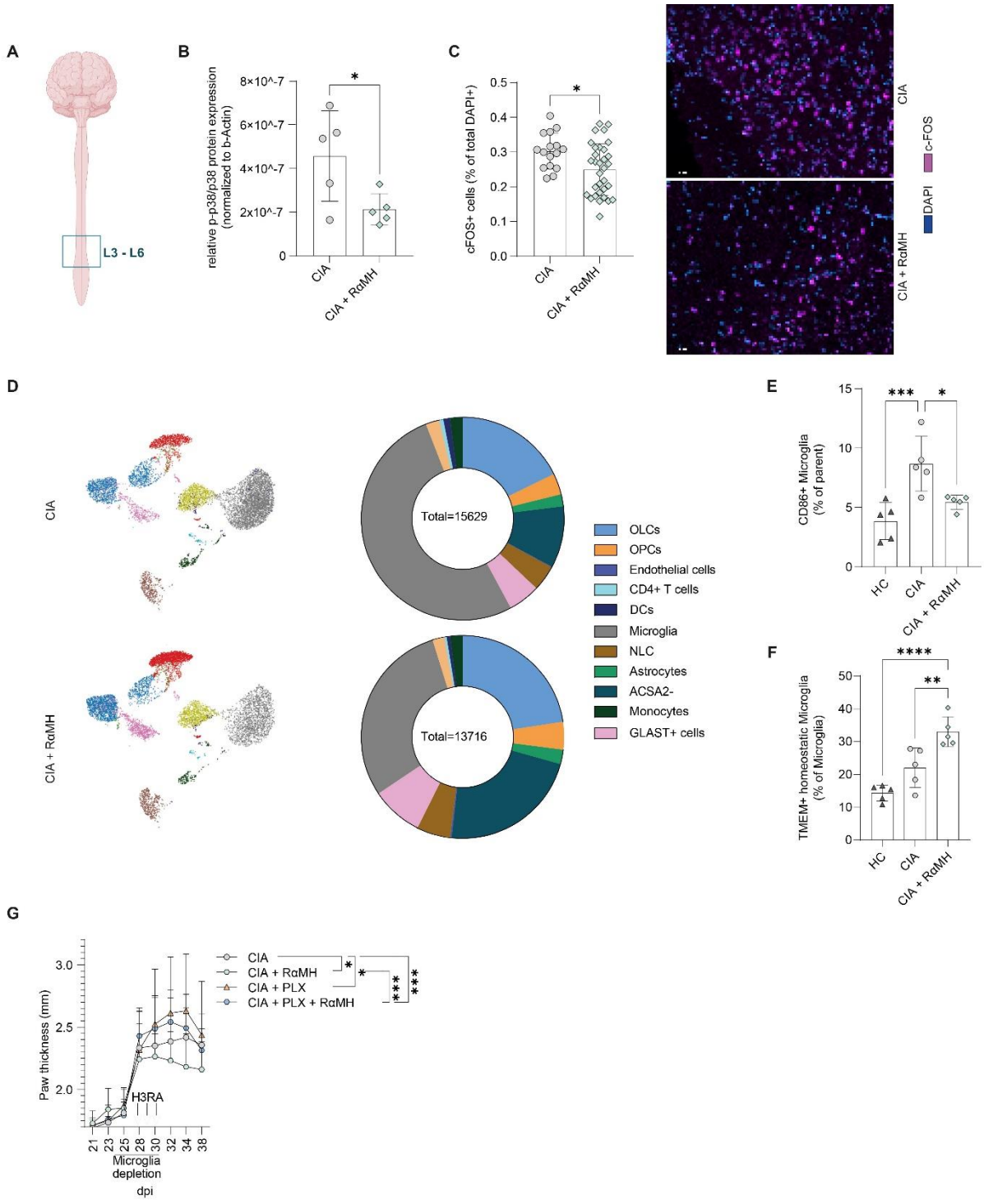

716

717 **Figure 4: Microglia depletion impairs histamine's pro-resolving effects**

718 **(A)** Visual representation of the analysed L3-L6 area of the spinal cord. This overview was

719 generated using BioRender. **(B)** Quantification of phosphorylated p38 protein expression in the

720 L3-L6 area of the spinal cord normalized on b-Actin (Western Blot). **(C)** Quantification of c-

721 Fos+ cells in the spinal cord and exemplary pictures of IF stained slides. **(D)** UMAP plot of

722 spinal cord cells isolated from CIA ± RαMH and donut chart (% of live cells) of the different
723 cell clusters analysed by spectral flow cytometry. **(E)** CD86+ inflammatory microglia. **(F)**
724 TMEM119+ homeostatic microglia. **(G)** Clinical arthritis score shown as paw thickness (mm)
725 of CIA mice with and without microglia depletion (25-30 dpi) ± RαMH at peak of disease. Data
726 are expressed as the mean ± sd. Statistical difference was determined by and Student's t-test
727 (B,C) One-way ANOVA (E,F) and One-way ANOVA of area under the curve (G). *$p < 0.05$;
728 **$p < 0.01$; ***$p < 0.001$; ****$p < 0.0001$. IF = Immunofluorescence.
729

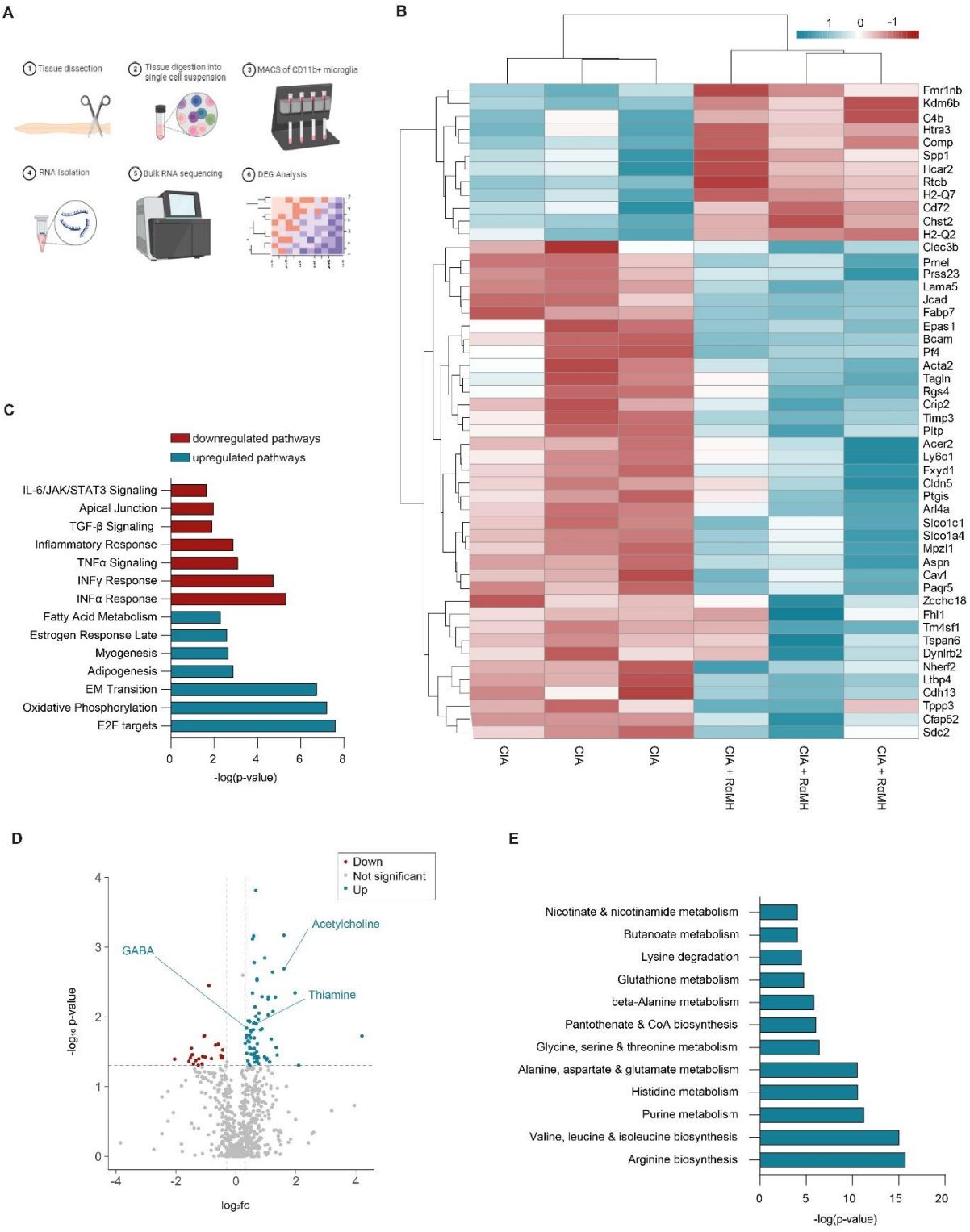

Figure 5: Oral H3R agonist treatment reverses the pro-inflammatory environment of the CNS

(A) Layout of the RNAseq experimental layout. This overview was generated using BioRender.

(B) Heatmap of the top 50 regulated genes in CD11b+ cells of the spinal cord (SC) in CIA mice

± RαMH. **(C)** Gene set enrichment of top 7 up- and downregulated hallmark pathways in the SC. **(D)** Volcano plot of untargeted metabolomics data of SC tissue supernatant of CIA mice ± RαMH. Cut-off were p-value < 0.05 and -0.3 < log2fc < 0.3. **(E)** Most upregulated metabolic pathways identified using MetaboAnalyst.

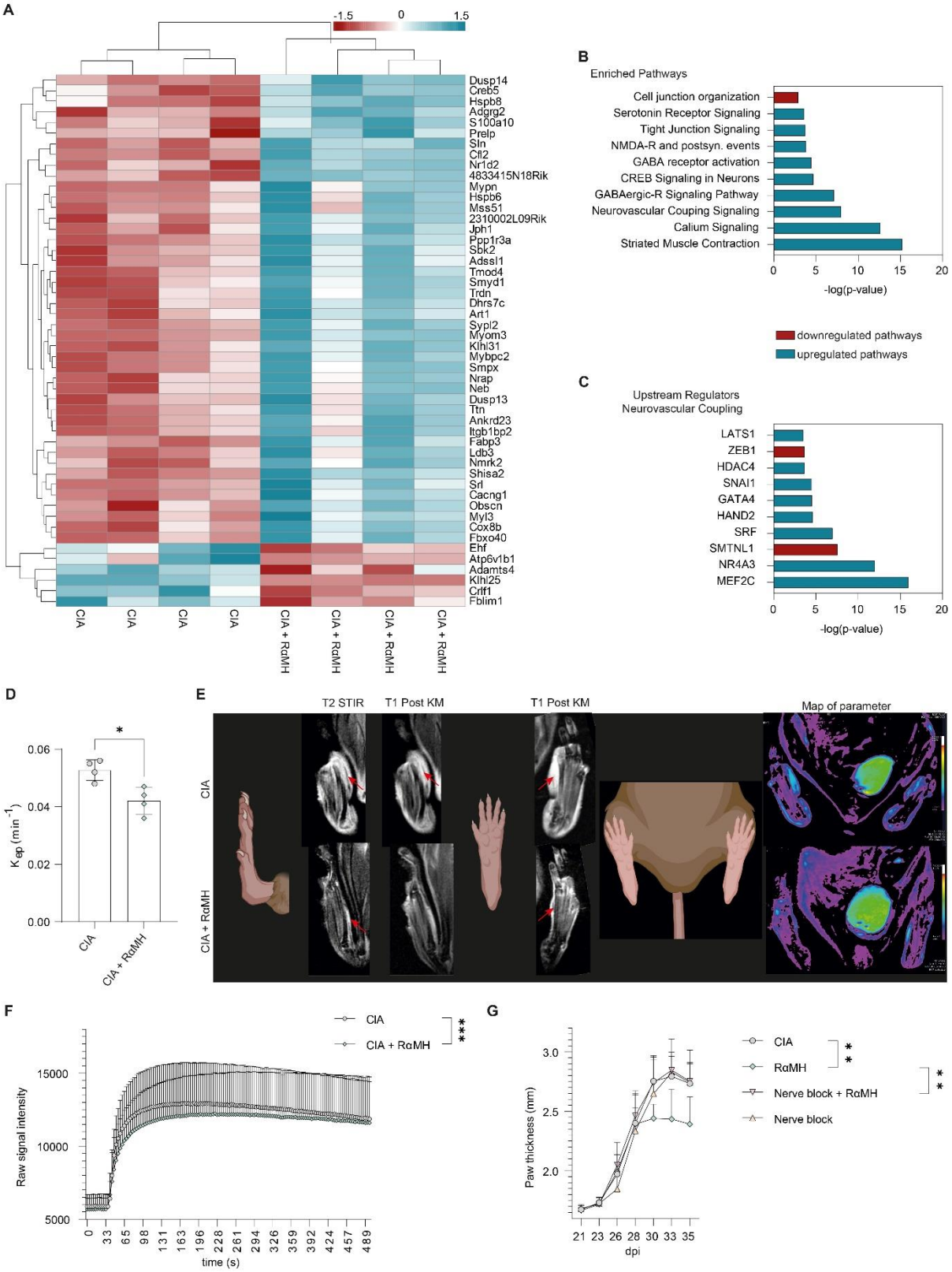

Figure 6: Intestinal H3R signaling reduces vascular leakage in inflamed paws

(A) Heatmap of the top 50 regulated genes in CD11b- cells of the Nervus plantaris (N.p.) in CIA mice ± RαMH. **(B)** Most enriched pathways identified by IPA analysis. **(C)** Top 10

upstream regulators of the enriched neurovascular coupling pathway (IPA). **(D)** K_{ep} (Transfer constant) in the paws of CIA mice ± RαMH on third treatment day. **(E)** Exemplary MRI pictures of T2 STIR, T1 POST KM, T1 POST KM and Map of parameter of CIA mice ± RαMH. **(F)** Raw signal intensity of DCE measurement over time of CIA mice ± RαMH. **(G)** Clinical arthritis score shown as paw thickness (mm) of CIA mice with/without QX-314 & bupivacaine induced nerve blockage ± RαMH (n=5) at peak of disease. Data are expressed as the mean ± sd. Statistical difference was determined by Student's t-test (D), Student's t-test of area under the curve (AUC) (F) and One-way ANOVA of AUC (G). *$p < 0.05$; **$p < 0.01$; ***$p < 0.001$

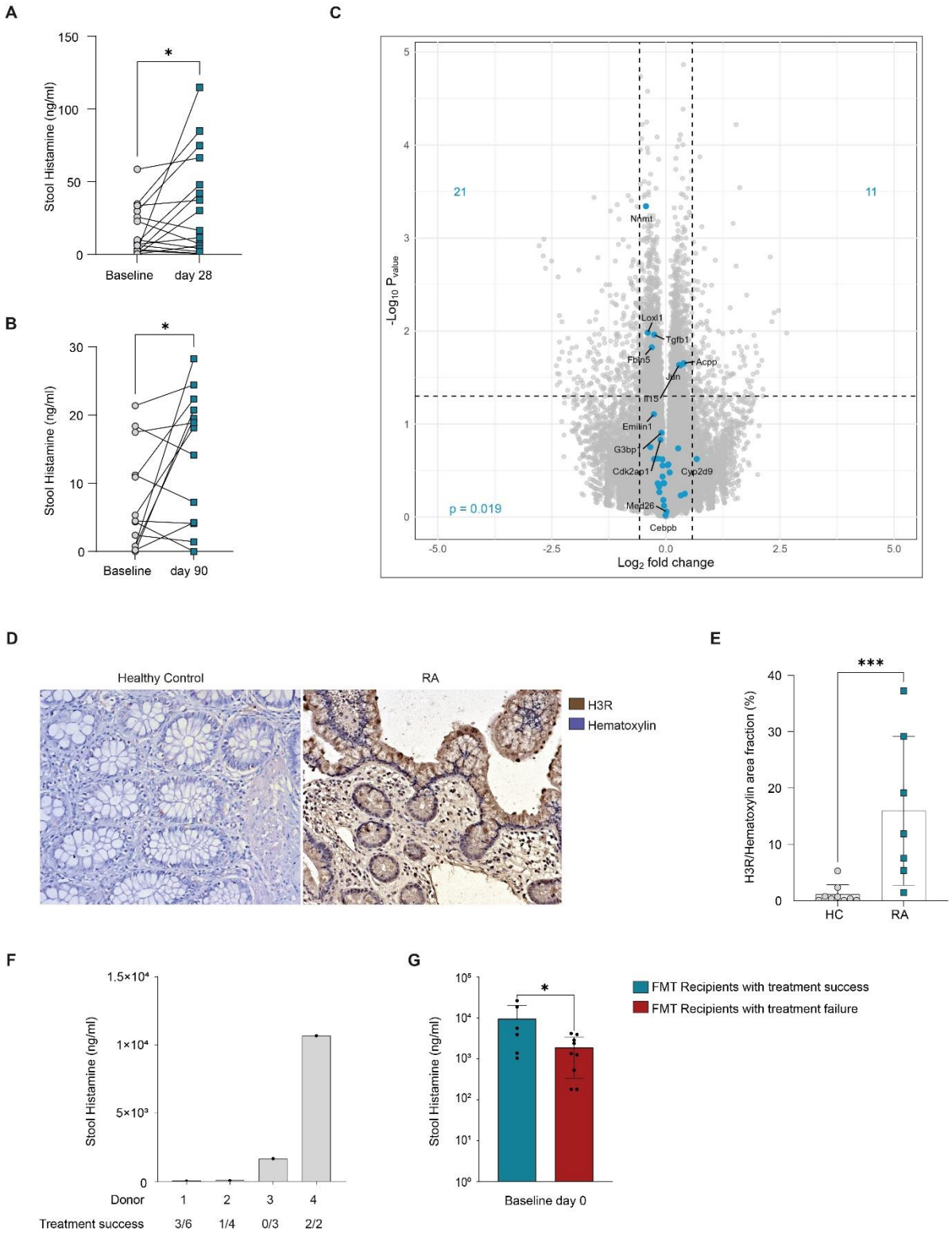

Figure 7: Propionate supplementation increases local histamine levels in RA and MS patients

(A) Histamine levels in stool extracts from RA patients before and after 28 days of propionate supplementation. **(B)** Histamine levels in stool extracts from MS patients before and after 90

days of propionate supplementation. **(C)** Volcano Plot of RNAseq data from ex vivo colon culture infused with stool samples from patients before and after 90 days of propionate supplementation. Overlay with pathway genes of H1R and H2R activation (GSEA pathway POS HISTAMINE RESPONSE NETWORK). **(D)** Exemplary pictures of histology staining of ileum biopsies from healthy controls (HC) or RA patients stained for H3R. **(E)** Quantification of histological H3R staining of ileum biopsies from patients and HC. **(F)** Histamine levels in the stool of 4 healthy donors processed to fecal microbiota transplants (FMT) (108). FMT was given to patients with active arthritis despite ongoing treatment with steady-state dose methotrexate. After 26 weeks patients were categorized as being either treatment failures or treatment responders, according to the European PsA recommendations (109). FMT products of Donor 1/2/3/4 were given to 6/4/3/2 patients, respectively. **(G)** Histamine was measured from stool of psoriatic arthritis (PsA) patients at baseline before FMT. Data are expressed as the mean ± sd. Statistical difference was determined by paired t test (A,B) and, Student's t-test (E). *$p < 0.05$; ***$p < 0.001$.

References

1. McInnes IB, Schett G. The pathogenesis of rheumatoid arthritis. N Engl J Med. 2011;365(23):2205-19.
2. Schaible HG, Straub RH. Function of the sympathetic supply in acute and chronic experimental joint inflammation. Auton Neurosci. 2014;182:55-64.
3. Waldburger JM, Firestein GS. Regulation of peripheral inflammation by the central nervous system. Curr Rheumatol Rep. 2010;12(5):370-8.
4. Abcouwer SF et al. Inflammatory resolution and vascular barrier restoration after retinal ischemia reperfusion injury. J Neuroinflammation. 2021;18(1):186.
5. Claesson-Welsh L et al. Permeability of the Endothelial Barrier: Identifying and Reconciling Controversies. Trends Mol Med. 2021;27(4):314-31.
6. Dong Y et al. Relationship between gut microbiota and rheumatoid arthritis: A bibliometric analysis. Front Immunol. 2023;14:1131933.
7. Maeda Y, Takeda K. Host-microbiota interactions in rheumatoid arthritis. Exp Mol Med. 2019;51(12):1-6.
8. Holers VM et al. Rheumatoid arthritis and the mucosal origins hypothesis: protection turns to destruction. Nat Rev Rheumatol. 2018;14(9):542-57.
9. Zaiss MM et al. The gut-joint axis in rheumatoid arthritis. Nat Rev Rheumatol. 2021;17(4):224-37.
10. Nerurkar L et al. Rheumatoid arthritis and depression: an inflammatory perspective. Lancet Psychiatry. 2019;6(2):164-73.
11. VanDyke MM et al. Anxiety in rheumatoid arthritis. Arthritis Rheum. 2004;51(3):408-12.
12. McDowell B et al. Prevalence of cognitive impairment in patients with rheumatoid arthritis: a cross sectional study. BMC Psychiatry. 2022;22(1):777.
13. Levine JD et al. Contribution of sensory afferents and sympathetic efferents to joint injury in experimental arthritis. J Neurosci. 1986;6(12):3423-9.

14. Sluka KA et al. Joint inflammation is reduced by dorsal rhizotomy and not by sympathectomy or spinal cord transection. Ann Rheum Dis. 1994;53(5):309-14.
15. Boyle DL et al. Regulation of peripheral inflammation by spinal p38 MAP kinase in rats. PLoS Med. 2006;3(9):e338.
16. Boyle DL et al. Spinal adenosine receptor activation inhibits inflammation and joint destruction in rat adjuvant-induced arthritis. Arthritis Rheum. 2002;46(11):3076-82.
17. Waldburger JM et al. Acetylcholine regulation of synoviocyte cytokine expression by the alpha7 nicotinic receptor. Arthritis Rheum. 2008;58(11):3439-49.
18. Rajasekaran N et al. Histidine decarboxylase but not histamine receptor 1 or 2 deficiency protects from K/BxN serum-induced arthritis. Int Immunol. 2009;21(11):1263-8.
19. Cowden JM et al. The histamine H4 receptor mediates inflammation and Th17 responses in preclinical models of arthritis. Ann Rheum Dis. 2014;73(3):600-8.
20. Nent E et al. Histamine 4 receptor plays an important role in auto-antibody-induced arthritis. Int Immunol. 2013;25(7):437-43.
21. Kim KW et al. Histamine and Histamine H4 Receptor Promotes Osteoclastogenesis in Rheumatoid Arthritis. Sci Rep. 2017;7(1):1197.
22. Grandi D et al. Immunolocalization of histamine H3 receptors on endocrine cells in the rat gastrointestinal tract. Histol Histopathol. 2008;23(7):789-98.
23. Kidd M et al. Autoregulation of enterochromaffin-like cell histamine secretion via the histamine 3 receptor subtype. Yale J Biol Med. 1996;69(1):9-19.
24. Bellono NW et al. Enterochromaffin Cells Are Gut Chemosensors that Couple to Sensory Neural Pathways. Cell. 2017;170(1):185-98 e16.
25. Honkisz-Orzechowska E et al. Anti-inflammatory effects of new human histamine H(3) receptor ligands with flavonoid structure on BV-2 neuroinflammation. Inflamm Res. 2023;72(2):181-94.
26. Teuscher C et al. Central histamine H3 receptor signaling negatively regulates susceptibility to autoimmune inflammatory disease of the CNS. Proc Natl Acad Sci U S A. 2007;104(24):10146-51.

824 27. Landete JM et al. Updated molecular knowledge about histamine biosynthesis by bacteria. Crit
825 Rev Food Sci Nutr. 2008;48(8):697-714.
826 28. Barcik W et al. Immune regulation by histamine and histamine-secreting bacteria. Curr Opin
827 Immunol. 2017;48:108-13.
828 29. Lucas S et al. Short-chain fatty acids regulate systemic bone mass and protect from pathological
829 bone loss. Nat Commun. 2018;9(1):55.
830 30. Haghikia A et al. Dietary Fatty Acids Directly Impact Central Nervous System Autoimmunity via the
831 Small Intestine. Immunity. 2015;43(4):817-29.
832 31. Stoll MA-O et al. Akkermansia muciniphila is permissive to arthritis in the K/BxN mouse model of
833 arthritis. (1476-5470 (Electronic)).
834 32. Aoki S. Rheumatoid arthritis and enteric bacteria. Japanese Journal of Rheumatology.
835 1999;9(4):325-52.
836 33. van Baarlen P et al. Regulation of intestinal homeostasis and immunity with probiotic lactobacilli.
837 Trends in Immunology. 2013;34(5):208-15.
838 34. Charlet R et al. Bacteroides thetaiotaomicron and Lactobacillus johnsonii modulate intestinal
839 inflammation and eliminate fungi via enzymatic hydrolysis of the fungal cell wall. Scientific
840 Reports. 2020;10(1):11510.
841 35. Jia D-J-C et al. Lactobacillus johnsonii alleviates colitis by TLR1/2-STAT3 mediated CD206+
842 macrophagesIL-10 activation. Gut Microbes. 2022;14(1):2145843.
843 36. Zhang YA-O et al. Caecal infusion of the short-chain fatty acid propionate affects the microbiota
844 and expression of inflammatory cytokines in the colon in a fistula pig model. (1751-7915
845 (Electronic)).
846 37. Dempsey E, Corr SC. Lactobacillus spp. for Gastrointestinal Health: Current and Future
847 Perspectives. Front Immunol. 2022;13:840245.
848 38. Thomas CM et al. Histamine derived from probiotic Lactobacillus reuteri suppresses TNF via
849 modulation of PKA and ERK signaling. PLoS One. 2012;7(2):e31951.

850 39.Barcik W et al. Bacterial secretion of histamine within the gut influences immune responses within
851 the lung. Allergy. 2019;74(5):899-909.
852 40.Leurs R et al. The histamine H3 receptor: from gene cloning to H3 receptor drugs. Nat Rev Drug
853 Discov. 2005;4(2):107-20.
854 41.Panula P. Chapter 23 - Histamine receptors, agonists, and antagonists in health and disease. In:
855 Swaab DF, Kreier F, Lucassen PJ, Salehi A, Buijs RM, editors. Handbook of Clinical Neurology. 180:
856 Elsevier; 2021. p. 377-87.
857 42.Arrang JM et al. Highly potent and selective ligands for histamine H3-receptors. Nature.
858 1987;327(6118):117-23.
859 43.Kitbunnadaj R et al. Identification of 4-(1H-Imidazol-4(5)-ylmethyl)pyridine (Immethridine) as a
860 Novel, Potent, and Highly Selective Histamine H3 Receptor Agonist. Journal of Medicinal
861 Chemistry. 2004;47(10):2414-7.
862 44.Zaiss MM et al. The Intestinal Microbiota Contributes to the Ability of Helminths to Modulate
863 Allergic Inflammation. (1097-4180 (Electronic)).
864 45.Sander LE et al. Selective expression of histamine receptors H1R, H2R, and H4R, but not H3R, in
865 the human intestinal tract. Gut. 2006;55(4):498-504.
866 46.Yissachar N et al. An Intestinal Organ Culture System Uncovers a Role for the Nervous System in
867 Microbe-Immune Crosstalk. Cell. 2017;168(6):1135-48 e12.
868 47.Joo JY et al. Stimulus-specific combinatorial functionality of neuronal c-fos enhancers. Nat
869 Neurosci. 2016;19(1):75-83.
870 48.Breunig E et al. Histamine excites neurones in the human submucous plexus through activation of
871 H1, H2, H3 and H4 receptors. The Journal of Physiology. 2007;583(2):731-42.
872 49.Evaldsson C et al. Anti-inflammatory effects of exogenous uridine in an animal model of lung
873 inflammation. International Immunopharmacology. 2007;7(8):1025-32.
874 50.Jeengar MK et al. Uridine Ameliorates Dextran Sulfate Sodium (DSS)-Induced Colitis in Mice.
875 Scientific Reports. 2017;7(1):3924.

51. Mejía-Toiber J et al. d-β-Hydroxybutyrate Prevents Glutamate-Mediated Lipoperoxidation and Neuronal Damage Elicited during Glycolysis Inhibition In Vivo. Neurochemical Research. 2006;31(12):1399-408.
52. Choi JW et al. Uridine Protects Cortical Neurons from Glucose Deprivation-Induced Death: Possible Role of Uridine Phosphorylase. Journal of Neurotrauma. 2008;25(6):695-707.
53. Jin L-W et al. The ketone body β-hydroxybutyrate shifts microglial metabolism and suppresses amyloid-β oligomer-induced inflammation in human microglia. The FASEB Journal. 2023;37(11):e23261.
54. Kim S-Y et al. Activation of p38 MAP kinase in the rat dorsal root ganglia and spinal cord following peripheral inflammation and nerve injury. NeuroReport. 2002;13(18).
55. Svensson CI et al. Activation of p38 mitogen-activated protein kinase in spinal microglia is a critical link in inflammation-induced spinal pain processing. (0022-3042 (Print)).
56. Rigaud M et al. Species and strain differences in rodent sciatic nerve anatomy: implications for studies of neuropathic pain. Pain. 2008;136(1-2):188-201.
57. Jie Z et al. Microglia promote autoimmune inflammation via the noncanonical NF-kappaB pathway. Sci Adv. 2021;7(36):eabh0609.
58. Montilla A et al. Microglia and meningeal macrophages depletion delays the onset of experimental autoimmune encephalomyelitis. Cell Death Dis. 2023;14(1):16.
59. Bellver-Landete V et al. Microglia are an essential component of the neuroprotective scar that forms after spinal cord injury. Nat Commun. 2019;10(1):518.
60. Janova H et al. Microglia ablation alleviates myelin-associated catatonic signs in mice. J Clin Invest. 2018;128(2):734-45.
61. De Schepper S et al. Perivascular cells induce microglial phagocytic states and synaptic engulfment via SPP1 in mouse models of Alzheimer's disease. Nat Neurosci. 2023;26(3):406-15.
62. McNamara NB et al. Microglia regulate central nervous system myelin growth and integrity. Nature. 2023;613(7942):120-9.

63. Parrott JM et al. Altered inflammatory response in FMRP-deficient microglia. iScience. 2021;24(11):103293.
64. Tsuchihashi R et al. Upregulation of IFN-beta induced by Sema4D-dependent partial Erk1/2 inhibition promotes NO production in microglia. Biochem Biophys Res Commun. 2020;521(4):827-32.
65. Kelley JM et al. Does gamma-aminobutyric acid (GABA) influence the development of chronic inflammation in rheumatoid arthritis? J Neuroinflammation. 2008;5:1.
66. van Maanen MA et al. Stimulation of nicotinic acetylcholine receptors attenuates collagen-induced arthritis in mice. Arthritis Rheum. 2009;60(1):114-22.
67. Medeiros RCN et al. Thiamine Deficiency Modulates p38(MAPK) and Heme Oxygenase-1 in Mouse Brain: Association with Early Tissue and Behavioral Changes. Neurochem Res. 2020;45(4):940-55.
68. Shan C et al. L-arginine metabolism inhibits arthritis and inflammatory bone loss. Annals of the Rheumatic Diseases. 2024;83(1):72.
69. Appelboom T Fau - Mandelbaum I et al. Purine enzyme levels in rheumatoid arthritis. (0315-162X (Print)).
70. Wu B, Zhao TV et al. Mitochondrial aspartate regulates TNF biogenesis and autoimmune tissue inflammation. Nat Immunol. 2021;22(12):1551-62.
71. Ronzano R et al. Microglia-neuron interaction at nodes of Ranvier depends on neuronal activity through potassium release and contributes to remyelination. Nat Commun. 2021;12(1):5219.
72. Binstadt BA et al. Particularities of the vasculature can promote the organ specificity of autoimmune attack. Nat Immunol. 2006;7(3):284-92.
73. Kwok CHT et al. Role of Primary Afferents in Arthritis Induced Spinal Microglial Reactivity. Front Immunol. 2021;12:626884.
74. Stangenberg L et al. Denervation protects limbs from inflammatory arthritis via an impact on the microvasculature. Proc Natl Acad Sci U S A. 2014;111(31):11419-24.

75. Deczkowska A et al. Mef2C restrains microglial inflammatory response and is lost in brain ageing in an IFN-I-dependent manner. Nat Commun. 2017;8(1):717.
76. Martinez-Gonzalez J et al. NR4A3: A Key Nuclear Receptor in Vascular Biology, Cardiovascular Remodeling, and Beyond. Int J Mol Sci. 2021;22(21).
77. Duscha A et al. Propionic Acid Shapes the Multiple Sclerosis Disease Course by an Immunomodulatory Mechanism. Cell. 2020;180(6):1067-80.e16.
78. Duscha A et al. Propionic acid beneficially modifies osteoporosis biomarkers in patients with multiple sclerosis. Therapeutic Advances in Neurological Disorders. 2022;15:17562864221103935.
79. Dürholz K et al. Dietary Short-Term Fiber Interventions in Arthritis Patients Increase Systemic SCFA Levels and Regulate Inflammation. LID - 10.3390/nu12103207 [doi] LID - 3207. (2072-6643 (Electronic)).
80. Häger J et al. The Role of Dietary Fiber in Rheumatoid Arthritis Patients: A Feasibility Study. LID - 10.3390/nu11102392 [doi] LID - 2392. (2072-6643 (Electronic)).
81. Kragsnaes MS et al. Small Intestinal Permeability and Metabolomic Profiles in Feces and Plasma Associate With Clinical Response in Patients With Active Psoriatic Arthritis Participating in a Fecal Microbiota Transplantation Trial: Exploratory Findings From the FLORA Trial. ACR Open Rheumatol. 2023;5(11):583-93.
82. Chu C et al. Neuro-immune Interactions in the Tissues. Immunity. 2020;52(3):464-74.
83. Levine YA et al. Neurostimulation of the cholinergic anti-inflammatory pathway ameliorates disease in rat collagen-induced arthritis. PLoS One. 2014;9(8):e104530.
84. Marsal S et al. Non-invasive vagus nerve stimulation for rheumatoid arthritis: a proof-of-concept study. Lancet Rheumatol. 2021;3(4):e262-e9.
85. Thompson M, Bywaters EG. Unilateral rheumatoid arthritis following hemiplegia. Ann Rheum Dis. 1962;21(4):370-7.

86. Capellino S et al. Catecholamine-producing cells in the synovial tissue during arthritis: modulation of sympathetic neurotransmitters as new therapeutic target. Ann Rheum Dis. 2010;69(10):1853-60.
87. Harle P et al. An opposing time-dependent immune-modulating effect of the sympathetic nervous system conferred by altering the cytokine profile in the local lymph nodes and spleen of mice with type II collagen-induced arthritis. Arthritis Rheum. 2005;52(4):1305-13.
88. Harle P et al. An early sympathetic nervous system influence exacerbates collagen-induced arthritis via CD4+CD25+ cells. Arthritis Rheum. 2008;58(8):2347-55.
89. Kim SY et al. Activation of p38 MAP kinase in the rat dorsal root ganglia and spinal cord following peripheral inflammation and nerve injury. Neuroreport. 2002;13(18):2483-6.
90. Sorkin LS et al. Origins of antidromic activity in sensory afferent fibers and neurogenic inflammation. Semin Immunopathol. 2018;40(3):237-47.
91. Kane D et al. Protective effect of sensory denervation in inflammatory arthritis (evidence of regulatory neuroimmune pathways in the arthritic joint). Ann Rheum Dis. 2005;64(2):325-7.
92. Tracey KJ. The inflammatory reflex. Nature. 2002;420(6917):853-9.
93. Wang H et al. Nicotinic acetylcholine receptor alpha7 subunit is an essential regulator of inflammation. Nature. 2003;421(6921):384-8.
94. Prast H et al. Histaminergic neurons modulate acetylcholine release in the ventral striatum: role of H3 histamine receptors. Naunyn Schmiedebergs Arch Pharmacol. 1999;360(5):558-64.
95. van Maanen MA et al. Role of the cholinergic nervous system in rheumatoid arthritis: aggravation of arthritis in nicotinic acetylcholine receptor alpha7 subunit gene knockout mice. Ann Rheum Dis. 2010;69(9):1717-23.
96. Peng C et al. Alpha7 nAChR Expression Is Correlated with Arthritis Development and Inhibited by Sinomenine in Adjuvant-Induced Arthritic Rats. Evid Based Complement Alternat Med. 2019;2019:3759304.

976 97. Mossink B et al. Cadherin-13 is a critical regulator of GABAergic modulation in human stem-cell-
977 derived neuronal networks. Mol Psychiatry. 2022;27(1):1-18.
978 98. Shao FB et al. Anxiolytic effect of GABAergic neurons in the anterior cingulate cortex in a rat
979 model of chronic inflammatory pain. Mol Brain. 2021;14(1):139.
980 99. Tamura S et al. Expression and distribution of GABAergic system in rat knee joint synovial
981 membrane. Histol Histopathol. 2009;24(8):1009-19.
982 100. Tian J et al. Oral GABA treatment downregulates inflammatory responses in a mouse model of
983 rheumatoid arthritis. Autoimmunity. 2011;44(6):465-70.
984 101. Liu B et al. Serum metabolomics analysis of deficiency pattern and excess pattern in patients
985 with rheumatoid arthritis. Chin Med. 2022;17(1):71.
986 102. Sluka KA, Westlund KN. An experimental arthritis in rats: dorsal horn aspartate and glutamate
987 increases. Neurosci Lett. 1992;145(2):141-4.
988 103. Czapski GA, Strosznajder JB. Glutamate and GABA in Microglia-Neuron Cross-Talk in Alzheimer's
989 Disease. Int J Mol Sci. 2021;22(21).
990 104. Li L et al. Acetylcholine suppresses microglial inflammatory response via alpha7nAChR to protect
991 hippocampal neurons. J Integr Neurosci. 2019;18(1):51-6.
992 105. Matsushita T et al. Sustained microglial activation in the area postrema of collagen-induced
993 arthritis mice. Arthritis Res Ther. 2021;23(1):273.
994 106. Suss P et al. Chronic Peripheral Inflammation Causes a Region-Specific Myeloid Response in the
995 Central Nervous System. Cell Rep. 2020;30(12):4082-95 e6.
996 107. Lei F et al. CSF1R inhibition by a small-molecule inhibitor is not microglia specific; affecting
997 hematopoiesis and the function of macrophages. Proc Natl Acad Sci U S A. 2020;117(38):23336-
998 8.
999 108. Kragsnaes MS et al. Safety and efficacy of faecal microbiota transplantation for active peripheral
1000 psoriatic arthritis: an exploratory randomised placebo-controlled trial. Ann Rheum Dis.
1001 2021;80(9):1158-67.

109. Gossec L et al. EULAR recommendations for the management of psoriatic arthritis with pharmacological therapies: 2019 update. Ann Rheum Dis. 2020;79(6):700-12.